Copyright © 2011 Tech Science Press CMES, vol.81, no.1, pp.69-118, 2011

Development of T-Trefftz Four-Node Quadrilateral and Voronoi Cell Finite Elements for Macro- & Micromechanical Modeling of Solids

L. Dong[1] **and S. N. Atluri**[2]

Abstract: In this paper, we explore three different ways of developing T-Trefftz finite elements of quadrilateral as well as polygonal shapes. In all of these three approaches, in addition to assuming an inter-element compatible displacement field along the element boundary, an interior displacement field for each element is independently assumed as a linear combination of T-Trefftz trial functions. In addition, a characteristic length is defined for each element to scale the T-Trefftz modes, in order to avoid solving systems of ill-conditioned equations. The differences between these three approaches are that, the compatibility between the independently assumed fields at the boundary and in the interior, are enforced alternatively, using a two-field boundary variational principle, collocation, and the least squares method. The corresponding four-node quadrilateral elements with/without drilling degrees of freedom are developed, for modeling macrostructures of solids. These three approaches are also used to derive T-Trefftz Voronoi Cell Finite Elements (VCFEM), for micromechanical analysis of heterogeneous materials. Several two dimensional macro- & micromechanical problems are solved using these elements. Computational results demonstrate that the elements derived using the collocation method are very simple, accurate and computationally efficient. Because the elements derived by this approach are also not plagued by LBB conditions, which are almost impossible to be satisfied a priori, we consider this class of elements to be useful for engineering applications in micromechanical modeling of heterogeneous materials.

Keywords: T-Trefftz, finite element, variational principle, collocation, least squares, LBB conditions, drilling degree of freedom, VCFEM

[1] Department of Civil & Environmental Engineering, University of California, Irvine, leitingd@uci.edu

[2] Center for Aerospace Research & Education, University of California, Irvine

1 Introduction

Primal finite elements, which involve displacement-type of nodal shape functions, are widely accepted and applied in computer modeling of physical problems. This is because of their simplicity, efficiency, stability and established convergence. However, the disadvantages of these elements are also well-known, such as unsatisfactory performance in problems which involve constraints (shear/membrane/incompressibility locking), difficulty to satisfy higher-order continuity requirements (especially for plates and shells), sensitivity to mesh distortion, etc. Carefully formulated hybrid/mixed finite elements based on multi-field assumptions, on the other hand, can mitigate or even resolve such problems. Thus, since its early development in 1960s, numerous formulations of hybrid/mixed finite elements have been proposed and applied to various physical problems. However, these hybrid/mixed elements developed along the lines of [Pian (1964)] are also well-known to be prohibitively more computationally-expensive than their (displacement) primal counterparts.

The original version of the hybrid stress elements developed in [Pian (1964)] was based on the modified principle of minimum complementary energy, using an "a priori equilibrated" stress field in each element, and an inter-element compatible displacement field along the element boundary. However, this type of element is somehow useless when modeling geometrically nonlinear and dynamical problems, because an "a priori equilibrated" stress field is almost impossible to be found in these problems. From a more general point of view, [Atluri (1975)] developed a generalized variational principle by modifying the Hu-Washizu principle to accommodate the finite-discretized domain. By choosing to satisfy some conditions a priori and the others a posteriori, Atluri's variational principle can essentially be reduced to different versions of variational principles for developing various finite element models, including the hybrid stress element, the hybrid strain element, the hybrid displacement element, etc. And some of these variational principles were also extended to develop finite elements with drilling degrees of freedoms in [Iura and Atluri (1992); Cazzani and Atluri (1993)], and for geometrical as well as material nonlinear problems in [Atluri (1980)].

Besides their applications in two-dimensional and three-dimensional solid mechanics, hybrid/mixed finite element methods were also demonstrated to be advantageous in other types of physical problems. For example, [Bratianu and Atluri (1983); Ying and Atluri (1983)] developed mixed finite elements for modeling Stokes flows, which eliminate incompressibility locking without resolving to selective reduced-order integrations. [Ghosh and Mallett (1994); Ghosh, Lee and Moorthy (1995)] developed Voronoi cell finite elements (VCFEM) and applied them to multi-scale analysis of structures composed of heterogeneous materials. [Jirousek

and Teodorescu (1982); Jirousek and Guex (1986)] developed hybrid Trefftz elements for two-dimensional solid mechanical problems and plate bending problems. [Cai, Paik and Atluri (2009 a,b); Cai, Paik and Atluri (2010); Cai, Paik and Atluri (2010); Zhu, Cai, Paik and Atluri (2010)] developed locking-free hybrid/mixed finite elements for modeling large rotation deformation of beams/rods/plates/shells considering von-Karman type of nonlinearity in co-rotational frames.

However, in spite of their widely recognized advantages, there are essentially two major drawbacks that have been limiting the engineering applications of hybrid/mixed finite elements. One is the increased computational burden caused by matrix inversion for each and every element, and the need to generate at least two different element matrices (**H** and **G**) through integrations over the element domain, in the process of developing the element stiffness matrix. The other is the questionable stability of finite element solutions. Matrix inversion is difficult to avoid as long as multi-field variational principles are used for element derivation. Regarding stability, [Babuska (1973); Brezzi (1974)] analyzed the existence, uniqueness, stability and convergence of problems with Lagrangian multipliers and established the so-called LBB conditions. Inability to satisfy the LBB conditions in general would plague the solvability and stability of hybrid/mixed finite element equations. [Rubinstein, Punch and Atluri (1983); Punch and Atluri (1984); Xue, Karlovitz and Atluri (1985)] used sophisticated group theory to develop guidelines for selecting independent fields which will satisfy the LBB conditions, under the condition that the element is undistorted. For an arbitrarily distorted element, to the best of the authors' knowledge, there is no rational way of satisfying LBB conditions a priori.

By noticing that previous hybrid/mixed models suffer from LBB conditions because multi-field variational principles use Lagrangian multipliers to enforce constraints, [Dong and Atluri (2011)] presented a simple approach to avoid LBB conditions when developing hybrid/mixed elements. The essential idea was to enforce the compatibility between independently assumed fields, using collocation or the least squares method, instead of using Lagrangian multipliers as in multi-field variational principles. Using this approach, hybrid/mixed four-node quadrilateral elements with independently assumed displacement and strain fields were developed, which were shown to be stable, locking-free, invariant, and computationally almost as efficient as primal finite elements. This approach was also applied to develop VCFEM, by assuming the element-interior displacement field as a linear combination of radial basis functions.

In this paper, we develop T-Trefftz four-node quadrilateral elements and T-Trefftz VCFEMs. For each element, in addition to assuming an inter-element compatible displacement field along the element boundary, an interior displacement field for each element is also independently assumed as a linear combination of T-Trefftz

trial functions. Three approaches are used alternatively to enforce the compatibility between independently assumed fields: a two-field boundary variational principle, the collocation method, and the least squares method. Elements developed using the two-field boundary variational principle are obviously plagued by LBB conditions, which are almost impossible to be satisfied a priori. On the other hand, elements developed using the other two approaches do not suffer from LBB conditions. Several macro- and micromechanical examples are also presented, to show the advantages and disadvantages of various elements.

The rest of this paper is organized as follows: in section 2, we introduce the characteristic-length-scaled T-Trefftz trial functions as the assumed interior displacement field; in section 3, we use three approaches to develop T-Trefftz four-node quadrilateral elements with/without drilling degree of freedoms; in section 4, we use the same three approaches to develop T-Trefftz VCFEMs for micromechanical modeling of materials; in section 5, we conduct numerical experiments and compare the performances of different elements; in section 6, we complete this paper with some concluding remarks.

2 Interior Displacement Field: T-Trefftz Trial Functions Scaled by a Characteristic Length

Consider a linear elastic solid undergoing infinitesimal elasto-static deformation. Cartesian coordinates x_i identify material particles in the solid. $\sigma_{ij}, \varepsilon_{ij}, u_i$ are Cartesian components of the stress tensor, strain tensor and displacement vector respectively. $\overline{f}_i, \overline{u}_i, \overline{t}_i$ are Cartesian components of the prescribed body force, boundary displacement and boundary traction vector. S_u, S_t are displacement boundary and traction boundary of the domain Ω. We use $()_{,i}$ to denote differentiation with respect to x_i. The equations of linear & angular momentum balance, constitutive equations, compatibility equations, and boundary conditions can be written as:

$$\sigma_{ij,j} + \overline{f}_i = 0 \text{ in } \Omega \tag{1}$$

$$\sigma_{ij} = \sigma_{ji} \text{ in } \Omega \tag{2}$$

$$\sigma_{ij} = E_{ijkl}\varepsilon_{kl} \text{ (or } \varepsilon_{ij} = C_{ijkl}\sigma_{kl}) \text{ in } \Omega \text{ for a linear elastic solid} \tag{3}$$

$$\varepsilon_{ij} = \frac{1}{2}(u_{i,j} + u_{j,i}) \equiv u_{(i,j)} \text{ in } \Omega \tag{4}$$

$$u_i = \bar{u}_i \text{ at } S_u \tag{5}$$

$$n_j \sigma_{ij} = \bar{t}_i \text{ at } S_t \tag{6}$$

Moreover, when the domain Ω is discretized into elements Ω_m with element boundary $\partial\Omega_m$, each element boundary can be divided into S_{um}, S_{tm}, ρ_m, which are intersections of $\partial\Omega_m$ with S_u, S_t and other element boundaries respectively. Then, in addition to satisfying (1)(2)(3)(4) in each Ω_m, satisfying (5)(6) at S_{um}, S_{tm}, displacement continuity and traction reciprocity conditions at each ρ_m should be considered:

$$u_i^+ = u_i^- \text{ at } \rho_m \tag{7}$$

$$(n_j\sigma_{ij})^+ + (n_j\sigma_{ij})^- = 0 \text{ at } \rho_m \tag{8}$$

In T-Trefftz elements derived in this study, we assume an interior displacement field u_i for each element, as well as an element boundary displacement field $\tilde{u}_i$, and enforce the compatibility between u_i and $\tilde{u}_i$ using either a two-field boundary variational principle, or collocation, or the least squares method, as seen in Fig. 1. u_i is assumed as a linear combination of T-Trefftz modes, which satisfy (1)(2)(3)(4) all together. For plane stress or plane strain problems where body force are negligible, these T-Trefftz modes can be generated by two complex potentials $\phi(z)$ and $\chi(z)$, see [Muskhelishvil (1954), Timoshenko and Goodier (1970)]:

$$\begin{aligned} u_1(z) &= Re\left[\kappa\phi(z) - z\overline{\phi'(z)} - \overline{\chi'(z)}\right]/2G \\ u_2(z) &= Im\left[\kappa\phi(z) - z\overline{\phi'(z)} - \overline{\chi'(z)}\right]/2G \end{aligned} \tag{9}$$

In (9), $z = x_1 + ix_2$ with $i = \sqrt{-1}$. $Re[]$ and $Im[]$ denote the real and imaginary part of a complex variable. G and κ are defined as:

$$\begin{aligned} \kappa &= \begin{cases} 3-4\nu & \text{for plane strain problems} \\ (3-\nu)/(1+\nu) & \text{for plane stress problems} \end{cases} \\ G &= \frac{E}{2(1+\nu)} \end{aligned} \tag{10}$$

where E, ν are the Young's modulus and Poisson ratio respectively.

For ease of numerical implementation, a set of polynomial functions $\phi(z)$ and $\chi'(z)$ are of particular interest:

$$\begin{aligned} \phi(z) &= \sum_{n=0}^{\infty} \left(i\alpha_n^1 + \alpha_n^2\right) z^n \\ \chi'(z) &= \sum_{n=0}^{\infty} \left(i\alpha_n^3 + \alpha_n^4\right) z^n \end{aligned} \tag{11}$$

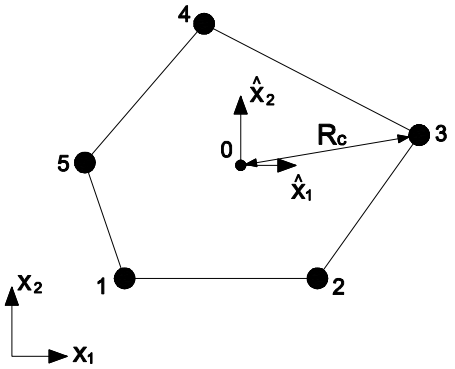

Figure 1: The concept of characteristic length

However, similar to what is frequently encountered in T-Trefftz methods, a system of ill-conditioned equations is to be solved in order to enforce the compatibility between u_i and $\tilde{u}_i$. This is because of the exponential growth of the term z^n with respect to the order n. [Liu (2007a, 2007b)] introduced the concept of characteristic length to scale the T-Trefftz modes for Laplace equations. Since this concept successfully resolved the ill-conditioned nature of Trefftz method for Laplace equations, it is also applied in this study, in the context of plane stress/strain solid mechanics.

Consider an arbitrary element as shown in Fig. 1. The coordinates of the nodes are $(x_1^k, x_2^k), k = 1,2...,N$. A local Cartesian coordinate system with the polygon center (x_1^c, x_2^c) as origin, is denoted as $\hat{x}_1 - \hat{x}_2$. $\hat{x}_1, \hat{x}_2$ are defined as:

$$\begin{aligned} &\hat{x}_1 = (x_1 - x_1^c)/R_c \\ &\hat{x}_2 = (x_2 - x_2^c)/R_c \\ &\quad \text{with } R_c = \max_k \sqrt{(x_1^k - x_1^c)^2 + (x_2^k - x_2^c)^2}\ k = 1,2...,N \end{aligned} \tag{12}$$

so that the T-Trefftz modes are scaled as:

$$\begin{aligned} &u_1(\hat{z}) = Re\left[\kappa\phi(\hat{z}) - z\overline{\phi'(\hat{z})} - \overline{\chi'(\hat{z})}\right]/2G \\ &u_2(\hat{z}) = Im\left[\kappa\phi(\hat{z}) - z\overline{\phi'(\hat{z})} - \overline{\chi'(\hat{z})}\right]/2G \\ &\quad \text{with } \hat{z} = \hat{x}_1 + i\hat{x}_2 \end{aligned} \tag{13}$$

where $\phi(\hat{z})$ and $\chi'(\hat{z})$ have the same form as $\phi(z)$ and $\chi'(z)$ defined in (11).

By adopting such a characteristic length R_c scaled local T-complete functions, $|\hat{z}^n|$ is confined between 0 and 1 for any point within the element or along element boundaries. Therefore the resulting systems of equations are well-conditioned, and can be easily solved without using any further regularization techniques.

For a specific n, taking one of $\alpha_n^1, \alpha_n^2, \alpha_n^3, \alpha_n^4$ to be 1, and the others to be 0, we obtain different T-Trefftz modes which are n^{th} order polynomials, denoted as $\mathbf{T}_n^1, \mathbf{T}_n^2, \mathbf{T}_n^3, \mathbf{T}_n^4$:

$$\begin{aligned}
2G\mathbf{T}_n^1 &= \begin{Bmatrix} ReZ_n^1 \\ ImZ_n^1 \end{Bmatrix} \text{ with } Z_n^1 = i\kappa\hat{z}^n + in\hat{z}\bar{\hat{z}}^{n-1} \\
2G\mathbf{T}_n^2 &= \begin{Bmatrix} ReZ_n^2 \\ ImZ_n^2 \end{Bmatrix} \text{ with } Z_n^2 = \kappa\hat{z}^n - n\hat{z}\bar{\hat{z}}^{n-1} \\
2G\mathbf{T}_n^3 &= \begin{Bmatrix} ReZ_n^3 \\ ImZ_n^3 \end{Bmatrix} \text{ with } Z_n^3 = i\bar{\hat{z}}^n \\
2G\mathbf{T}_n^4 &= \begin{Bmatrix} ReZ_n^4 \\ ImZ_n^4 \end{Bmatrix} \text{ with } Z_n^4 = -\bar{\hat{z}}^n
\end{aligned} \tag{14}$$

For convenience of illustration, we still use x_1, x_2, z in the rest of this paper, instead of using $\hat{x}_1, \hat{x}_2, \hat{z}$, to denote the T-Trefftz modes, implying that a characteristic length R_c is already used for each element to scale the T-Trefftz modes.

We should point out that, for $n = 0$, $\mathbf{T}_0^1, \mathbf{T}_0^3$ both represent the rigid-body translational mode in the direction x_2, while $\mathbf{T}_0^2, \mathbf{T}_0^4$ both represent the rigid-body translational mode in the direction x_1. For $n = 1$, $\mathbf{T}_1^1$ represent the rigid-body rotational mode in the plane $x_1 - x_2$. All other modes are independent non-rigid-body modes. In addition, if one assumes u_i to be a linear combination of the first m independent T-Trefftz modes, such a displacement field is rotationally invariant if m is an even number. For example, if one assume u_i to be a linear combination of $T_0^3, T_0^4, T_1^1, T_1^2, ..., T_2^5, T_2^6$, such an assumption is rotationally invariant. On the other hand, if one assume u_i to be a linear combination of $T_0^3, T_0^4, T_1^1, T_1^2, ..., T_2^5$, such an assumption is not rotationally invariant.

It should be noted that, introducing the characteristic length $R_c$may not have significant advantages for four-node quadrilateral elements. But for higher-order elements and VCFEMs with large number of nodes, scaling T-Trefftz modes with the characteristic length R_c is almost necessary, because much higher order T-Trefftz modes are needed.

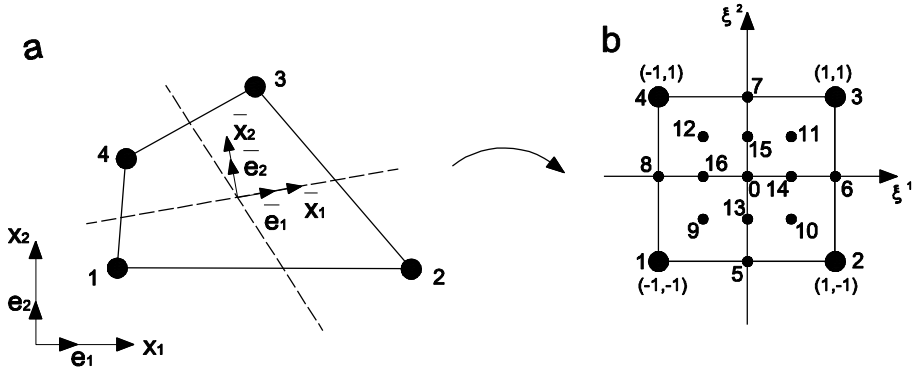

Figure 2: Four-node quadrilateral element: (a) Cartesian coordinates (b) curvilinear (non-dimensional) coordinates

3 T-Trefftz Four-Node Quadrilateral Elements with/without Drilling Degrees of Freedom

3.1 Elements without Drilling Degrees of Freedom

Consider a four-node quadrilateral element as seen in Fig. 2. Some points are marked for convenience of illustration, including: center point (which is also the point for a one-point Gauss integration) 0; nodal points 1, 2, 3, 4; edge midpoints 5, 6, 7, 8; 2 by 2 Gaussian integration points 9, 10, 11, 12; 1 by 2 Gaussian integration points 13, 15; 2 by 1 Gaussian integration points 14, 16.

The element boundary displacement field $\tilde{u}_i$ is assumed as a linear field along each edge, and can be extrapolated to the whole element domain as:

$$x_i = x_i^{(1)} N^{(1)}(\xi^\gamma) + x_i^{(2)} N^{(2)}(\xi^\gamma) + x_i^{(3)} N^{(3)}(\xi^\gamma) + x_i^{(4)} N^{(4)}(\xi^\gamma) \tag{15}$$

$$\tilde{u}_i = \tilde{u}_i^{(1)} N^{(1)}(\xi^\gamma) + \tilde{u}_i^{(2)} N^{(2)}(\xi^\gamma) + \tilde{u}_i^{(3)} N^{(3)}(\xi^\gamma) + \tilde{u}_i^{(4)} N^{(4)}(\xi^\gamma) \tag{16}$$

which is the assumed displacement field of a four-node isoparametric quadrilateral element, with:

$$\begin{aligned} N^{(1)} &= (1-\xi^1)(1-\xi^1)/4 \\ N^{(2)} &= (1+\xi^1)(1-\xi^1)/4 \\ N^{(3)} &= (1+\xi^1)(1+\xi^1)/4 \\ N^{(4)} &= (1+\xi^1)(1-\xi^1)/4 \end{aligned} \tag{17}$$

It is well known that such a displacement field includes five non-rigid-body modes: two extensional modes, two bending modes, and a shear mode. However, the shear mode is locked with the two bending modes, therefore (16) cannot represent pure bending modes. In order to develop T-Trefftz elements which avoid locking, we independently assume an uncoupled element interior displacement field :

$$\begin{aligned}\left\{u_1 \quad u_2\right\}^T = & \alpha_6 \mathbf{T}_0^3 + \alpha_7 \mathbf{T}_0^4 + \alpha_8 \mathbf{T}_1^1 \\ & + \alpha_1 \left(\mathbf{T}_1^2 - 2\mathbf{T}_1^4\right)/4 + \alpha_2 \left(\mathbf{T}_1^2 + 2\mathbf{T}_1^4\right)/4 + \alpha_3 \mathbf{T}_1^3 \\ & + \alpha_4 \left(\mathbf{T}_2^3 - \mathbf{T}_2^1\right)/8 + \alpha_5 \left(\mathbf{T}_2^2 + \mathbf{T}_2^4\right)/8\end{aligned} \tag{18}$$

This leads to a stress field:

$$\begin{Bmatrix}\sigma_{11}\\ \sigma_{22}\\ \sigma_{12}\end{Bmatrix} = \begin{Bmatrix}\alpha_1 + \alpha_4 x_2\\ \alpha_2 + \alpha_5 x_1\\ \alpha_3\end{Bmatrix} = \begin{bmatrix}1 & 0 & 0 & x_2 & 0\\ 0 & 1 & 0 & 0 & x_1\\ 0 & 0 & 1 & 0 & 0\end{bmatrix} \boldsymbol{\alpha} \tag{19}$$

It can be clearly seen from (18)(19) that, α_1, α_2 represent the two constant extensional modes, α_3 represents the constant shear mode, α_4, α_5 represent the two pure bending modes, and $\alpha_6, \alpha_7, \alpha_8$ represent the three rigid-body modes.

Adopting matrix and vector notation, we have:

$$\begin{aligned}\mathbf{u} &= \mathbf{N}\boldsymbol{\alpha} \text{ in } \Omega_m\\ \boldsymbol{\varepsilon} &= \mathbf{B}\mathbf{q} \text{ in } \Omega_m\\ \boldsymbol{\sigma} &= \mathbf{D}\boldsymbol{\varepsilon} = \mathbf{S}\boldsymbol{\alpha} \text{ in } \Omega_m\\ \mathbf{t} &= \mathbf{n}\boldsymbol{\sigma} = \mathbf{R}\boldsymbol{\alpha} \text{ at } \partial\Omega_m\\ \tilde{\mathbf{u}} &= \tilde{\mathbf{N}}\mathbf{q} \text{ in } \Omega_m\\ \tilde{\boldsymbol{\varepsilon}} &= \tilde{\mathbf{B}}\mathbf{q} \text{ in } \Omega_m\\ \tilde{\boldsymbol{\sigma}} &= \mathbf{D}\tilde{\boldsymbol{\varepsilon}} = \tilde{\mathbf{S}}\boldsymbol{\alpha} \text{ in } \Omega_m\\ \tilde{\mathbf{t}} &= \mathbf{n}\tilde{\boldsymbol{\sigma}} = \tilde{\mathbf{R}}\boldsymbol{\alpha} \text{ at } \partial\Omega_m\end{aligned} \tag{20}$$

There are several ways of relating $\boldsymbol{\alpha}$ to $\mathbf{q}$, which lead to different T-Trefftz finite elements. Firstly, one can relate $\alpha_1 - \alpha_5$ to the vector $\mathbf{q}$ using a two-field variational principle—the boundary variational principle, see [Atluri and Grannell (1978)] ($\alpha_6 - \alpha_8$ should be eliminated from (18) when using this method because they do not contribute to the strain energy stored in the element). Such a two-field variational principle states that, given an element interior u_i satisfying (1)(2)(3)(4) a priori, an continuous inter-element $\tilde{u}_i$ satisfying (5), conditions (6)(7)(8) can be derived from stationarity conditions of the following functional:

$$\pi_1(u_i, \tilde{u}_i) = \sum_m \left\{ \int_{\Omega m} \frac{1}{2} t_i u_i d\Omega - \int_{\partial\Omega_m} t_i \tilde{u}_i dS + \int_{S_{tm}} \bar{t}_i \tilde{u}_i dS \right\} \tag{21}$$

where t_i is derived from u_i:

$$t_i = n_j E_{ijkl} u_{(k,l)} \tag{22}$$

The stationarity conditions of (21) can be seen to be only on element and global boundaries:

$$\begin{aligned} &n_j E_{ijkl} u_{(k,l)} = \bar{t}_i \text{ at } S_{tm} \\ &u_i^+ = u_i^- = \tilde{u}_i \text{ at } \rho_m \\ &\left(n_j E_{ijkl} u_{(k,l)}\right)^+ + \left(n_j E_{ijkl} u_{(k,l)}\right)^- = 0 \text{ at } \rho_m \end{aligned} \tag{23}$$

Substituting assumed $u_i, \tilde{u}_i$ into the boundary variational principle (21), we have:

$$\begin{aligned} &\delta\pi_1(\boldsymbol{\alpha}, \mathbf{q}) = 0 \\ &= \delta \sum_m \left(\frac{1}{2} \boldsymbol{\alpha}^T \mathbf{H} \boldsymbol{\alpha} - \mathbf{q}^T \mathbf{G}^T \boldsymbol{\alpha} + \mathbf{q}^T \mathbf{Q} \right) \\ &= \sum_m \left(\delta\boldsymbol{\alpha}^T \mathbf{H} \boldsymbol{\alpha} - \delta\mathbf{q}^T \mathbf{G}^T \boldsymbol{\alpha} - \delta\boldsymbol{\alpha}^T \mathbf{G}\mathbf{q} + \delta\mathbf{q}^T \mathbf{Q} \right) \\ &\mathbf{G} = \int_{\partial\Omega m} \mathbf{R}^T \tilde{\mathbf{N}} dS = \int_{\Omega m} \mathbf{S}^T \tilde{\mathbf{B}} dS \\ &\mathbf{H} = \int_{\partial\Omega m} \mathbf{R}^T \mathbf{N} dS = \int_{\Omega m} \mathbf{S}^T \mathbf{D}^{-1} \mathbf{S}^T d\Omega \\ &\mathbf{Q} = \int_{Stm} \tilde{\mathbf{N}}^T \bar{\mathbf{t}} dS \end{aligned} \tag{24}$$

This leads to:

$$\delta\boldsymbol{\alpha}^T \mathbf{H} \boldsymbol{\alpha} = \delta\boldsymbol{\alpha}^T \mathbf{G}\mathbf{q} \tag{25}$$

$$\delta\mathbf{q}^T \mathbf{G}^T \boldsymbol{\alpha} - \delta\mathbf{q}^T \mathbf{Q} = 0 \tag{26}$$

And the finite element equations are:

$$\sum_m \left(\delta\mathbf{q}^T \mathbf{K}\mathbf{q} - \delta\mathbf{q}^T \mathbf{Q} \right) = \sum_m \left(\delta\mathbf{q}^T \mathbf{G}^T \mathbf{H}^{-1} \mathbf{G}\mathbf{q} - \delta\mathbf{q}^T \mathbf{Q} \right) = 0 \tag{27}$$

We denote the elements derived this way as Q4-TT-BVP (boundary variational principle). From a weighted-residual point of view, in Q4-TT-BVP, $\boldsymbol{\alpha}$ are related to $\mathbf{q}$ by enforcing the compatibility of u_i and $\tilde{u}_i$ in a weak sense using test function $\delta\mathbf{t} = \mathbf{R}\delta\boldsymbol{\alpha}$. However, this clearly involves Lagrangian multipliers and therefore Q4-TT-BVP suffers from LBB conditions, which are almost impossible to be satisfied a priori.

We also point out that, although derived from different approaches, it can be shown that the stiffness matrix of Q4-TT-BVP is the same as the hybrid stress element developed in [Pian 1964], using (19) as the independent stress field assumption. In this study, we denote the hybrid stress element presented in [Pian (1964)] as Q4-HS-PCE (the principle of complementary energy). For a long time, Q4-HS-PCE is considered to be able to satisfy LBB conditions, because the element stiffness matrix of Q4-HS-PCE for a square element is rank-sufficient [Pian and Chen (1983)]. This, however, does not hold for arbitrary distorted element. In section 5, we will give an example where both Q4-TT-BVP and Q4-HS-PCE generate the same rank-deficient matrices.

In order to avoid LBB conditions, [Dong and Atluri (2011)] proposed to enforce the independent assumed fields in a strong sense at several pre-selected collocation points, and thus relate the independently assumed field to nodal displacements. For this particular problem, because $\tilde{u}_i$ can be extrapolated to the whole element domain, there are at least two ways of relating $\boldsymbol{\alpha}$ to $\mathbf{q}$ using the collocation method. Firstly, we can enforce the compatibility between u_i and $\tilde{u}_i$ at four nodes $x_i^{(k)}, k = 1,2,3,4$. This leads to:

$$u_i(x_i^{(k)}, \boldsymbol{\alpha}) = \tilde{u}_i(x_i^{(k)}, \mathbf{q}),\ k = 1,2,3,4 \tag{28}$$

We denote this as Q4-TT-C1.

We can also enforce the compatibility of the stress fields derived from u_i and $\tilde{u}_i$ respectively, say σ_{ij} and $\tilde{\sigma}_{ij}$, at several preselected collocation points, ($\alpha_6 - \alpha_8$ should be eliminated in this case). For example, use the 1 by 2 Gaussian integration points $x_i^{(13)}, x_i^{(15)}$ as collocation points forσ_{11}, 2 by 1 Gaussian integration points $x_i^{(14)}, x_i^{(16)}$ as collocation points for σ_{22}, and $x_i^{(0)}$ the point for one-point Gaussian integration as the collocation point for σ_{12}, we obtain five equations for solving $\alpha_1 - \alpha_5$ ($\alpha_6 - \alpha_8$ should be eliminated from (18) in this case):

$$\begin{aligned}
&\sigma_{11}(x_i^{(k)}, \boldsymbol{\alpha}) = \tilde{\sigma}_{11}(x_i^{(k)}, \mathbf{q}),\ k = 13,15 \\
&\sigma_{22}(x_i^{(k)}, \boldsymbol{\alpha}) = \tilde{\sigma}_{22}(x_i^{(k)}, \mathbf{q}),\ k = 14,16 \\
&\sigma_{12}(x_i^{(k)}, \boldsymbol{\alpha}) = \tilde{\sigma}_{12}(x_i^{(k)}, \mathbf{q}),\ k = 0
\end{aligned} \tag{29}$$

We denote this as Q4-TT-C2.

Using either (28) or (29), we can obtain:

$$\boldsymbol{\alpha} = \mathbf{C}\mathbf{q} \tag{30}$$

In this case, u_i already satisfy (1)(2)(3)(4), and are related to $\tilde{u}_i$ using collocation

method which satisfy (5)(7), conditions (6)(8) can be derived from:

$$\pi_2(u_i) = \sum_m \left\{ \int_{\Omega m} \frac{1}{2} t_i u_i d\Omega - \int_{S_{tm}} \bar{t}_i u_i dS \right\} \tag{31}$$

which leads to Euler-Lagrange equations:

$$\begin{aligned} &n_j E_{ijkl} u_{(k,l)} = \bar{t}_i \text{ at } S_{tm} \\ &\left(n_j E_{ijkl} u_{(k,l)}\right)^+ + \left(n_j E_{ijkl} u_{(k,l)}\right)^- = 0 \text{ at } \rho_m \end{aligned} \tag{32}$$

Substituting u_i into (31) , we obtain finite element equations for Q4-TT-C1,2:

$$\sum_m \left(\delta \mathbf{q}^T \mathbf{K}\mathbf{q} - \delta \mathbf{q}^T \mathbf{Q}\right) = \sum_m \left(\delta \mathbf{q}^T \mathbf{C}^T \mathbf{H}\mathbf{C}\mathbf{q} - \delta \mathbf{q}^T \mathbf{Q}\right) = 0 \tag{33}$$

Finally, when the number of collocation points is increased to a limit of infinity, it is equivalent to enforcing the compatibility between u_i and $\tilde{u}_i$, or σ_{ij} and $\tilde{\sigma}_{ij}$ using the least squares method, namely minimizing one of the following functionals:

$$\begin{aligned} e_1(\boldsymbol{\alpha}, \mathbf{q}) &= \int_{\partial\Omega_m} (u_i - \tilde{u}_i)(u_i - \tilde{u}_i) dS \\ &= \int_{\partial\Omega_m} \left(\boldsymbol{\alpha}^T \mathbf{N}^T \mathbf{N}\boldsymbol{\alpha} - 2\boldsymbol{\alpha}^T \mathbf{N}^T \tilde{\mathbf{N}}\mathbf{q} + \mathbf{q}^T \tilde{\mathbf{N}}^T \tilde{\mathbf{N}}\mathbf{q}\right) dS \\ &= \boldsymbol{\alpha}^T \mathbf{U}_1 \boldsymbol{\alpha} - 2\boldsymbol{\alpha}^T \mathbf{V}_1 \mathbf{q} + \mathbf{q}^T \mathbf{W}_1 \mathbf{q} \end{aligned} \tag{34}$$

$$\begin{aligned} e_2(\boldsymbol{\alpha}, \mathbf{q}) &= \int_{\partial\Omega_m} (\sigma_{ij} - \tilde{\sigma}_{ij})(\sigma_{ij} - \tilde{\sigma}_{ij}) dS \\ &= \int_{\partial\Omega_m} \left(\boldsymbol{\alpha}^T \mathbf{S}^T \mathbf{S}\boldsymbol{\alpha} - 2\boldsymbol{\alpha}^T \mathbf{S}^T \tilde{\mathbf{S}}\mathbf{q} + \mathbf{q}^T \tilde{\mathbf{S}}^T \tilde{\mathbf{S}}\mathbf{q}\right) dS \\ &= \boldsymbol{\alpha}^T \mathbf{U}_2 \boldsymbol{\alpha} - 2\boldsymbol{\alpha}^T \mathbf{V}_2 \mathbf{q} + \mathbf{q}^T \mathbf{W}_2 \mathbf{q} \end{aligned} \tag{35}$$

Parameters $\alpha_6 - \alpha_8$ should be eliminated when e_2 is used because they do not contribute to σ_{ij}.

To minimize e_1 or e_2 for a fixed $\mathbf{q}$, we have:

$$\boldsymbol{\alpha} = \mathbf{L}\mathbf{q} \tag{36}$$

Substituting u_i into (31), we obtain finite element equations:

$$\sum_m \left(\delta \mathbf{q}^T \mathbf{K}\mathbf{q} - \delta \mathbf{q}^T \mathbf{Q}\right) = \sum_m \left(\delta \mathbf{q}^T \mathbf{L}^T \mathbf{H}\mathbf{L}\mathbf{q} - \delta \mathbf{q}^T \mathbf{Q}\right) = 0 \tag{37}$$

We denote elements developed this way as Q4-TT-LS1 and Q4-TT-LS2 (least squares).

Because Q4-TT-C1,2 and Q4-TT-LS1,2 do not involve Lagrangian multipliers, these elements do not suffer from LBB conditions. Considering that it is almost impossible to satisfy LBB conditions a priori for arbitrarily distorted elements, we consider this as a significant advantage of Q4-TT -C1,2 and Q4-TT-LS1,2 over Q4-TT-BVP, as well as Q4-HS-PCE.

Moreover, in addition to the integration along the element boundary to find $\mathbf{H}$, Q4-TT-BVP requires integration of $\mathbf{G}$ along the element boundary, and Q4-TT-LS requires integration of both $\mathbf{U}_1$ and $\mathbf{V}_1$ (or $\mathbf{U}_2$ and $\mathbf{V}_2$) along the element boundary. On the other hand, the only integration involved in the development of stiffness matrix of Q4-TT-C1,2 is the evaluation of $\mathbf{H}$. Therefore, Q4-TT-C1,2 are expected to be computationally the most efficient among these elements.

3.2 Elements with Four Drilling Degrees of Freedom

Including drilling DOFs in finite elements has been extensively studied. One major reason is that, it demonstrates significant advantages to combine a plate bending element with a membrane element with drilling DOFs to model plates/shells.

There are mainly two approaches of introducing drilling DOFs in membrane elements. One is to simply relate the displacement field of the element with drilling DOFs to a higher-order element, and use the principle of minimum potential energy to derive finite element equations, see [Allman (1984)]. For example, one can develop a four-node quadrilateral element with drillings DOFs, by relating its displacement field to that of an eight-node quadrilateral element. In spite of its simplicity, Allman's type of element has several disadvantages: one has to play special tricks to eliminate kinematic modes for each element; the rotation field is not true rotation, etc.

Another approach is developed by [Iura and Atluri (1992)]. In this approach, the displacement field and the rotation field in each element are both assumed, and the finite element equations can be developed using a variational principle involving both the displacement and rotation fields. Using this approach, elements which display no kinematic modes, and have true rotation field can be developed. The convergence of the finite element solutions using this approach is also proved in [Hughes and Brezzi (1989)]. This approach is also extended to develop elements with drilling DOFs and independently assumed asymmetric stress field in [Cazzani and Atluri (1993)]. In this study, we develop T-Trefftz elements with drilling DOFs using the approach developed by [Iura and Atluri (1992); Cazzani and Atluri (1993)].

Firstly, we present the displacement-type variational principle derived in [Iura and

Atluri (1992); Cazzani and Atluri (1993)]:

$$\begin{aligned}\pi_3(u_i,\theta_i) = \sum_m \left\{ \int_{\Omega m} \left[\frac{1}{2} E_{ijkl} u_{(i,j)} u_{(k,l)} - \bar{f}_i u_i \right] d\Omega - \int_{S_{tm}} \bar{t}_i u_i dS \right\} \\ + \int_{\Omega_m} \frac{\alpha}{2} \left(\theta_{ij} + \frac{1}{2} u_{j,i} - \frac{1}{2} u_{i,j} \right) \left(\theta_{ij} + \frac{1}{2} u_{j,i} - \frac{1}{2} u_{i,j} \right) d\Omega \end{aligned} \tag{38}$$

α is a user-defined parameter which should be strictly positive. In [Iura and Atluri (1992); Cazzani and Atluri (1993)], it was shown that solutions are insensitive to α. In this study, we use $\alpha = G$.

The stationarity conditions of (38) are:

$$\begin{aligned} &\left(E_{ijkl} u_{(k,l)}\right)_{,j} + \bar{f}_i = 0 \text{ in } \Omega_m \\ &\frac{\alpha}{2} \left(\theta_{ij} + \frac{1}{2} u_{j,i} - \frac{1}{2} u_{i,j} \right) = 0 \text{ in } \Omega_m \\ &n_j E_{ijkl} u_{(k,l)} = \bar{t}_i \text{ at } S_{tm} \\ &u_i^+ = u_i^- \text{ at } \rho_m \\ &\left(n_j E_{ijkl} u_{(k,l)}\right)^+ + \left(n_j E_{ijkl} u_{(k,l)}\right)^- = 0 \text{ at } \rho_m \end{aligned} \tag{39}$$

The second equation in (39) can be considered as the definition of θ_{ij}, the rotation in plane $x_i - x_j$, which satisfies $\theta_{ij} = -\theta_{ji}$. For two-dimensional problem, only one rotation is to be considered, i.e. $\theta = \theta_{12} = -\theta_{21}$. Alternatively, this can also be interpreted as the condition of angular momentum balance, where $s_{ij} = \alpha \left(\theta_{ij} + \frac{1}{2} u_{j,i} - \frac{1}{2} u_{i,j} \right)$ can be considered as the anti-symmetric portion of a priori asymmetric stress tensor t^*_{ij}, such that:

$$\begin{aligned} &t^*_{ij} = \sigma_{ij} + s_{ij}; \\ &\sigma_{ij} = \sigma_{ji}; \\ &s_{ij} = -s_{ji} \end{aligned} \tag{40}$$

Therefore, this displacement-type variational principle was also naturally extended by [Iura and Atluri (1992); Cazzani and Atluri (1993)] to accommodate independently assumed asymmetric stress field t^*_{ij} (equivalent to assumed σ_{ij} and s_{ij}), leading to a Ressiner-type variational principle:

$$\begin{aligned}\pi_4(t^*_{ij},u_i,\theta_i) = \sum_m \left\{ \int_{\Omega m} \left[\sigma_{ij} u_{(i,j)} - \frac{1}{2} C_{ijkl} \sigma_{ij} \sigma_{kl} - \bar{f}_i u_i \right] d\Omega - \int_{S_{tm}} \bar{t}_i u_i dS \right\} \\ + \sum_m \left\{ \int_{\Omega m} \left[s_{ij} \left(\theta_{ij} + \frac{1}{2} u_{j,i} - \frac{1}{2} u_{i,j} \right) - \frac{1}{2\alpha} s_{ij} s_{ij} \right] d\Omega \right\} \end{aligned} \tag{41}$$

which leads to Euler-Lagrange equations:

$$\begin{aligned}
&\left[E_{ijkl}u_{(k,l)}\right]_{,j}+\bar{f}_i=0 \text{ in } \Omega_m\\
&\frac{\alpha}{2}\left(\theta_{ij}+\frac{1}{2}u_{j,i}-\frac{1}{2}u_{i,j}\right)=0 \text{ in } \Omega_m\\
&n_jE_{ijkl}u_{(k,l)}=\bar{t}_i \text{ at } S_{tm}\\
&u_i^+=u_i^-=\tilde{u}_i \text{ at } \rho_m\\
&\left(n_jE_{ijkl}u_{(k,l)}\right)^+ + \left(n_jE_{ijkl}u_{(k,l)}\right)^- = 0 \text{ at } \rho_m
\end{aligned} \tag{42}$$

Similar to (21), we consider an element interior u_i satisfying (1)(2)(3)(4) a priori, an inter-element compatible $\tilde{u}_i$ satisfying (5), as well as an independently assumed rotation field θ_{ij}, a boundary variational principle involving both displacement and rotation field can also be derived:

$$\begin{aligned}
\pi_5(u_i,\tilde{u}_i,\theta_{ij}) = -\sum_m \left\{\int_{\Omega m}\frac{1}{2}t_iu_i d\Omega - \int_{\partial\Omega_m} t_i\tilde{u}_i dS + \int_{S_{tm}}\bar{t}_i\tilde{u}_i dS\right\}\\
+\int_{\Omega m}\frac{\alpha}{2}\left(\theta_{ij}+\frac{1}{2}u_{j,i}-\frac{1}{2}u_{i,j}\right)\left(\theta_{ij}+\frac{1}{2}u_{j,i}-\frac{1}{2}u_{i,j}\right)d\Omega
\end{aligned} \tag{43}$$

which leads to Euler-Lagrange equations:

$$\begin{aligned}
&\frac{\alpha}{2}\left(\theta_{ij}+\frac{1}{2}u_{j,i}-\frac{1}{2}u_{i,j}\right)=0 \text{ in } \Omega_m\\
&n_jE_{ijkl}u_{(k,l)}=\bar{t}_i \text{ at } S_{tm}\\
&u_i^+=u_i^-=\tilde{u}_i \text{ at } \rho_m\\
&\left(n_jE_{ijkl}u_{(k,l)}\right)^+ + \left(n_jE_{ijkl}u_{(k,l)}\right)^- = 0 \text{ at } \rho_m
\end{aligned} \tag{44}$$

Because (43) clearly involves Lagrangian multipliers, T-Trefftz elements with drilling DOFs developed using (43) are plagued by LBB conditions. However, (38) does not involve any Lagrangian multiplier. Similar to Q4-TT-C1,2 and Q4-TT-LS1,2, elements without involving LBB conditions can be developed by enforcing the compatibility of independently assumed displacement fields using collocation or the least squares method, and substituting the displacement and rotation fields in to variational principle (38).

Now we develop four-node quadrilateral elements with drilling DOFs using (38) or (43). From these two variational principles, we can see that θ does not need to be continuous over Ω, and can be assumed to be independent in each element. If this is the case, drilling DOFs can be eliminated locally using static condensation. However, in engineering applications where drilling DOFs are needed (for example,

when modeling plates/shells), it is usually desirable to preserve the drilling DOFs at each node. Therefore, in this study, we assume drilling DOFs to be continuous over Ω:

$$\theta = \theta^{(1)}N^{(1)}(\xi^\gamma) + \theta^{(2)}N^{(2)}(\xi^\gamma) + \theta^{(3)}N^{(3)}(\xi^\gamma) + \theta^{(4)}N^{(4)}(\xi^\gamma) \tag{45}$$

To make the element with drilling DOFs to present a similar property of an 8-node quadrilateral element, we assume $\tilde{u}_i$ to be Allman-type of displacement field.

$$\begin{aligned}\tilde{u}_i = {} & \tilde{u}_i^{(1)}N^{(1)}(\xi^\gamma) + \tilde{u}_i^{(2)}N^{(2)}(\xi^\gamma) + \tilde{u}_i^{(3)}N^{(3)}(\xi^\gamma) + \tilde{u}_i^{(4)}N^{(4)}(\xi^\gamma) \\ & + \theta^{(1)}M_i^{(1)}(\xi^\gamma) + \theta^{(2)}M_i^{(2)}(\xi^\gamma) + \theta^{(3)}M_i^{(3)}(\xi^\gamma) + \theta^{(4)}M_i^{(4)}(\xi^\gamma)\end{aligned} \tag{46}$$

where shape function for $\theta^{(k)}$ are defined by relating them to the shape functions of the 8-node quadrilateral element:

$$\begin{Bmatrix} M_1^{(k)} \\ M_2^{(k)} \end{Bmatrix} = \frac{1}{8}\begin{Bmatrix} -x_2^{(k+1)} + x_2^{(k)} \\ x_1^{(k+1)} - x_1^{(k)} \end{Bmatrix} NS^{(k)} - \frac{1}{8}\begin{Bmatrix} -x_2^{(k)} + x_2^{(k-1)} \\ x_1^{(k)} - x_1^{(k-1)} \end{Bmatrix} NS^{(k-1)} \tag{47}$$

$NS^{(k)}$ is the nodal shape function of the mid-edge node right after node k in a 8-node quadrilateral element, and $NS^{(k-1)}$ is the shape function of the mid-edge node right before node k. For example, $NS^{(1)}$ should be the nodal shape function of node 5 in an 8-node quadrilateral element as in Fig. 2, i.e.:

$$\begin{aligned} NS^{(1)} &= \left[1 - \left(\xi^1\right)^2\right]\left(1 - \xi^2\right)/2 \\ NS^{(2)} &= \left[1 - \left(\xi^2\right)^2\right]\left(1 + \xi^1\right)/2 \\ NS^{(3)} &= \left[1 - \left(\xi^1\right)^2\right]\left(1 + \xi^2\right)/2 \\ NS^{(4)} &= \left[1 - \left(\xi^2\right)^2\right]\left(1 - \xi^1\right)/2 \end{aligned} \tag{48}$$

In vector and matrix notation, we have:

$$\begin{aligned} &\tilde{\mathbf{u}} = \tilde{\mathbf{N}}_{\mathbf{q}}\mathbf{q} + \tilde{\mathbf{N}}_{\boldsymbol{\theta}}\boldsymbol{\theta} \text{ in } \Omega_m \\ &\tilde{\boldsymbol{\varepsilon}} = \tilde{\mathbf{B}}_{\mathbf{q}}\mathbf{q} + \tilde{\mathbf{B}}_{\boldsymbol{\theta}}\boldsymbol{\theta} \text{ in } \Omega_m \\ &\tilde{\boldsymbol{\sigma}} = \mathbf{D}\tilde{\boldsymbol{\varepsilon}} = \tilde{\mathbf{S}}_{\mathbf{q}}\mathbf{q} + \tilde{\mathbf{S}}_{\boldsymbol{\theta}}\boldsymbol{\theta} \text{ in } \Omega_m \\ &\tilde{\mathbf{t}} = \tilde{\mathbf{n}}\tilde{\boldsymbol{\sigma}} = \tilde{\mathbf{R}}_{\mathbf{q}}\mathbf{q} + \tilde{\mathbf{R}}_{\boldsymbol{\theta}}\boldsymbol{\theta} \text{ at } \partial\Omega_m \\ &\theta + \frac{1}{2}\tilde{u}_{1,2} - \frac{1}{2}\tilde{u}_{2,1} = \mathbf{E}_{\mathbf{q}}\mathbf{q} + \mathbf{E}_{\boldsymbol{\theta}}\boldsymbol{\theta} \text{ in } \Omega_m \end{aligned} \tag{49}$$

If we substitute the assumed $\tilde{u}_i, \theta_i$ into the displacement-type variational principle (38) with drilling DOFs, finite element equations can be obtained:

$$\sum_m \delta \begin{Bmatrix} \mathbf{q} \\ \boldsymbol{\theta} \end{Bmatrix}^T \left(\begin{bmatrix} \mathbf{k_{qq}} + \mathbf{K_{qq}} & \mathbf{k_{q\theta}} + \mathbf{K_{q\theta}} \\ \mathbf{k}_{\mathbf{q}\boldsymbol{\theta}}^T + \mathbf{K}_{\mathbf{q}\boldsymbol{\theta}}^T & \mathbf{k}_{\mathbf{q}\boldsymbol{\theta}}^T + \mathbf{K}_{\theta\theta} \end{bmatrix} \begin{Bmatrix} \mathbf{q} \\ \boldsymbol{\theta} \end{Bmatrix} - \begin{Bmatrix} \mathbf{Q_q} \\ \mathbf{Q}_\theta \end{Bmatrix} \right) = 0 \tag{50}$$

where

$$\begin{aligned}
\mathbf{K_{qq}} &= \int_{\Omega_m} \tilde{\mathbf{B}}_\mathbf{q}^T \mathbf{D} \tilde{\mathbf{B}}_\mathbf{q} d\Omega \\
\mathbf{K_{q\theta}} &= \int_{\Omega_m} \tilde{\mathbf{B}}_\mathbf{q}^T \mathbf{D} \tilde{\mathbf{B}}_{\boldsymbol{\theta}} d\Omega \\
\mathbf{K_{\theta\theta}} &= \int_{\Omega_m} \tilde{\mathbf{B}}_{\boldsymbol{\theta}}^T \mathbf{D} \tilde{\mathbf{B}}_{\boldsymbol{\theta}} d\Omega \\
\mathbf{k_{qq}} &= \frac{\alpha}{2} \int_{\Omega_m} \mathbf{E}_\mathbf{q}^T \mathbf{E_q} d\Omega \\
\mathbf{k_{q\theta}} &= \frac{\alpha}{2} \int_{\Omega_m} \mathbf{E}_\mathbf{q}^T \mathbf{E}_{\boldsymbol{\theta}} d\Omega \\
\mathbf{k}_{\theta\theta} &= \frac{\alpha}{2} \int_{\Omega_m} \mathbf{E}_\theta^T \mathbf{E}_{\boldsymbol{\theta}} d\Omega \\
\mathbf{Q_q} &= \int_{\Omega_m} \tilde{\mathbf{N}}_\mathbf{q}^T \bar{\mathbf{t}} d\Omega \\
\mathbf{Q}_\theta &= \int_{\Omega_m} \tilde{\mathbf{N}}_{\boldsymbol{\theta}}^T \bar{\mathbf{t}} d\Omega
\end{aligned} \tag{51}$$

We denote this element as Q4-D4.

To extend this element to accommodate an independently assumed T-Trefftz type of u_i, at least nine non-rigid-body T-Trefftz modes should be selected. However, in this case, there is no way to assume an uncoupled interior displacement field as in T-Trefftz elements, without drilling DOFs, derived in section 3.1. In this study, we assume the interior displacement field as:

$$\begin{aligned}
\begin{Bmatrix} u_1 & u_2 \end{Bmatrix}^T = {} & \alpha_{10} \mathbf{T}_0^3 + \alpha_{11} \mathbf{T}_0^4 + \alpha_{12} \mathbf{T}_1^1 \\
& + \alpha_1 \mathbf{T}_1^2 + \alpha_2 \mathbf{T}_1^3 + \alpha_3 \mathbf{T}_1^4 \\
& + \alpha_4 \mathbf{T}_2^1 + \alpha_5 \mathbf{T}_2^2 + \alpha_6 \mathbf{T}_2^3 + \alpha_7 \mathbf{T}_2^4 \\
& + \alpha_8 \mathbf{T}_3^1 + \alpha_9 \mathbf{T}_3^2
\end{aligned} \tag{52}$$

where $\alpha_1 - \alpha_9$ represents non-rigid-body modes and $\alpha_{10} - \alpha_{12}$ represents the 3 rigid-body modes.

Using matrix and vector notation, we have:

$$\begin{aligned}
&\mathbf{u} = \mathbf{N}\boldsymbol{\alpha} \text{ in } \Omega_m \\
&\boldsymbol{\varepsilon} = \mathbf{B}\mathbf{q} \text{ in } \Omega_m \\
&\boldsymbol{\sigma} = \mathbf{D}\boldsymbol{\varepsilon} = \mathbf{S}\boldsymbol{\alpha} \text{ in } \Omega_m \\
&\mathbf{t} = \mathbf{n}\boldsymbol{\sigma} = \mathbf{R}\boldsymbol{\alpha} \text{ at } \partial\Omega_m
\end{aligned} \tag{53}$$

Again, similar to Q4-TT-BVP, Q4-TT-C1,2, and Q4-TT-LS1,2, finite element equations can be developed using the following methods:

1. Substitute the assumed $u_i, \tilde{u}_i, \theta$ into variational principle (43) ($\alpha_{10} - \alpha_{12}$ should be eliminated in this case). We denote this element as Q4-D4-TT-BVP. The finite element equations of Q4-D4-TT-BVP are still in the same form of (50), by only changing the portion of stiffness matrix that is not related to α:

$$\begin{aligned}
&\sum_m \delta \begin{Bmatrix} \mathbf{q} \\ \boldsymbol{\theta} \end{Bmatrix}^T \left(\begin{bmatrix} \mathbf{k_{qq}} + \mathbf{K_{qq}} & \mathbf{k_{q\theta}} + \mathbf{K_{q\theta}} \\ \mathbf{k_{q\theta}^T} + \mathbf{K_{q\theta}^T} & \mathbf{k_{q\theta}^T} + \mathbf{K}_{\theta\theta} \end{bmatrix} \begin{Bmatrix} \mathbf{q} \\ \boldsymbol{\theta} \end{Bmatrix} - \begin{Bmatrix} \mathbf{Q_q} \\ \mathbf{Q}_\theta \end{Bmatrix} \right) = 0 \\
&\begin{bmatrix} \mathbf{K_{qq}} & \mathbf{K_{q\theta}} \\ \mathbf{K_{q\theta}^T} & \mathbf{K}_{\theta\theta} \end{bmatrix} = \mathbf{G}^T \mathbf{H}^{-1} \mathbf{G} \\
&\mathbf{G} = \int_{\partial\Omega m} \mathbf{R}^T \begin{bmatrix} \tilde{\mathbf{N}}_\mathbf{q} & \tilde{\mathbf{N}}_{\boldsymbol{\theta}} \end{bmatrix} dS = \int_{\Omega m} \mathbf{S}^T \begin{bmatrix} \tilde{\mathbf{B}}_\mathbf{q} & \tilde{\mathbf{B}}_{\boldsymbol{\theta}} \end{bmatrix} dS \\
&\mathbf{H} = \int_{\partial\Omega m} \mathbf{R}^T \mathbf{N} dS = \int_{\Omega m} \mathbf{S}^T \mathbf{D}^{-1} \mathbf{S}^T d\Omega
\end{aligned} \tag{54}$$

Q4-D4-TT-BVP are clearly plagued by LBB conditions.

2. Enforce the compatibility of u_i & $\tilde{u}_i$ or σ_{ij} & $\tilde{\sigma}_{ij}$ by collocation, and substitute u_i, θ to variational principle (38). We denote these two types of element as Q4-D4-TT-C1,2. Collocation points are selected in such a way:

- For Q4-D4-TT-C1, we collocate u_i at four nodal points 1, 2, 3, 4, and mid-edge points 5, 6, 7, 8.
- For Q4-D4-TT-C2, we collocate σ_{ij} at 2 by 2 Gaussian integration points 9, 10 ,11, 12, as well as the centroid 0, ($\alpha_{10} - \alpha_{12}$ should be eliminated in this case).

In either way, $\boldsymbol{\alpha}$ are related to $\mathbf{q}$, and the finite element equations are:

$$\begin{aligned}
&\sum_m \delta \begin{Bmatrix} \mathbf{q} \\ \boldsymbol{\theta} \end{Bmatrix}^T \left(\begin{bmatrix} \mathbf{k_{qq}} + \mathbf{K_{qq}} & \mathbf{k_{q\theta}} + \mathbf{K_{q\theta}} \\ \mathbf{k_{q\theta}^T} + \mathbf{K_{q\theta}^T} & \mathbf{k_{q\theta}^T} + \mathbf{K}_{\theta\theta} \end{bmatrix} \begin{Bmatrix} \mathbf{q} \\ \boldsymbol{\theta} \end{Bmatrix} - \begin{Bmatrix} \mathbf{Q_q} \\ \mathbf{Q}_\theta \end{Bmatrix} \right) = 0 \\
&\begin{bmatrix} \mathbf{K_{qq}} & \mathbf{K_{q\theta}} \\ \mathbf{K_{q\theta}^T} & \mathbf{K}_{\theta\theta} \end{bmatrix} = [\begin{bmatrix} \mathbf{C_q} & \mathbf{C_{\boldsymbol{\theta}}} \end{bmatrix}]^T \mathbf{H} [\begin{bmatrix} \mathbf{C_q} & \mathbf{C_{\boldsymbol{\theta}}} \end{bmatrix}] \\
&\boldsymbol{\alpha} = \mathbf{C_q}\mathbf{q} + \mathbf{C_{\boldsymbol{\theta}}}\boldsymbol{\theta} \text{ obtained by collocation}
\end{aligned} \tag{55}$$

3. Enforce the compatibility of u_i & $\tilde{u}_i$ or σ_{ij} & $\tilde{\sigma}_{ij}$ by the least squares method, minimize the functional in (34) or (35), relate u_i to nodal displacement vector $\mathbf{q}$, and substitute u_i, θ to variational principle (38). We denote these two types of elements as denoted as Q4-D4-TT-LS1,2. $\alpha_{10} - \alpha_{12}$ should be eliminated when e_2 is used.

In either way, $\boldsymbol{\alpha}$ are related to $\mathbf{q}$, and the finite element equations are modified as:

$$\begin{aligned}
&\sum_m \delta \begin{Bmatrix} \mathbf{q} \\ \boldsymbol{\theta} \end{Bmatrix}^T \left(\begin{bmatrix} \mathbf{k_{qq}} + \mathbf{K_{qq}} & \mathbf{k_{q\theta}} + \mathbf{K_{q\theta}} \\ \mathbf{k}_{\mathbf{q\theta}}^T + \mathbf{K}_{\mathbf{q\theta}}^T & \mathbf{k}_{\mathbf{q\theta}}^T + \mathbf{K}_{\theta\theta} \end{bmatrix} \begin{Bmatrix} \mathbf{q} \\ \boldsymbol{\theta} \end{Bmatrix} - \begin{Bmatrix} \mathbf{Q_q} \\ \mathbf{Q}_\theta \end{Bmatrix} \right) = 0 \\
&\begin{bmatrix} \mathbf{K_{qq}} & \mathbf{K_{q\theta}} \\ \mathbf{K}_{\mathbf{q\theta}}^T & \mathbf{K}_{\theta\theta} \end{bmatrix} = \begin{bmatrix} \mathbf{L_q} & \mathbf{L_\theta} \end{bmatrix}^T \mathbf{H} \begin{bmatrix} \mathbf{L_q} & \mathbf{L_\theta} \end{bmatrix}
\end{aligned} \tag{56}$$

$\boldsymbol{\alpha} = \mathbf{L_q q} + \mathbf{L_\theta \theta}$ obtained by the least square method

3.3 Remarks on Patch Test and Element Invariance

In [Dong and Atluri (2011)], it was pointed out that for hybrid/mixed elements developed using multi-field variational principles, the patch test can be passed if the assumed fields include constant strain modes and satisfy LBB conditions. For elements developed using collocation method or the least squares method, on the other hand, another condition is required to be satisfied:

$$\sum_m \int_{\Omega_m} \varepsilon_{ij}(\xi^{\gamma k}, \boldsymbol{\alpha}) d\Omega = \sum_m \int_{\Omega_m} \tilde{\varepsilon}_{ij}(\xi^{\gamma k}, \mathbf{q}) d\Omega \; \forall \; \boldsymbol{\alpha} = \mathbf{Cq} \text{ (or } \boldsymbol{\alpha} = \mathbf{Lq}) \tag{57}$$

or equivalently:

$$\sum_m \int_{\Omega_m} \sigma_{ij}(\xi^{\gamma k}, \boldsymbol{\alpha}) d\Omega = \sum_m \int_{\Omega_m} \tilde{\sigma}_{ij}(\xi^{\gamma k}, \mathbf{q}) d\Omega \; \forall \; \boldsymbol{\alpha} = \mathbf{Cq} \text{ (or } \boldsymbol{\alpha} = \mathbf{Lq}) \tag{58}$$

Therefore, it can be expected that TT-BVP can always pass the patch test, if the element stiffness matrix is rank-sufficient. TT-LS2 and TT-C2 would pass the patch test or give very small errors. However, the errors in the patch test for TT-C1 and TT-LS1 would be relatively large. Such an expectation is verified by numerical experiments in section 5.

In addition, since we always use incomplete T-Trefftz modes for these four-node quadrilateral elements, invariance is not ensured if element stiffness matrices are developed in the global Cartesian coordinate system $x_1 - x_2$. However, element invariance can be ensured by developing stiffness matrices in a local element-fixed coordinate system and transferring it back to the global Cartesian coordinate system. In this study, the following local Cartesian coordinate system $\bar{x}_1 - \bar{x}_2$ is selected. $\bar{\mathbf{e}}_\mathbf{1}$ is in the same direction of $\mathbf{g}_1$, the covariant base vector evaluated at point

0, and $\bar{\mathbf{e}}_2$ is obtained by rotating $\bar{\mathbf{e}}_1$ with respect to $\mathbf{e_3}$ counterclockwise 90°. Element stiffness matrices are developed in this local coordinate system $\bar{x}_1 - \bar{x}_2$, and transferred back to the global Cartesian coordinate system $x_1 - x_2$. Developed using such an approach, all the elements of TT-BVP, TT-C1,2, TT-LS1,2 are all ensured to be invariant.

4 T-Trefftz Voronoi Cell Finite Elements

[Ghosh and Mallett (1994); Ghosh, Lee and Moorthy (1995)] proposed the idea of discretizing the solution domain using Dirichlet tessellation, and developing corresponding Voronoi cell finite elements (VCFEM)/polygonal finite elements to solve problems of micromechanics of materials. However, the underlying theoretical foundation of the VCFEM proposed by [Ghosh and Mallett (1994); Ghosh, Lee and Moorthy (1995)] is the modified principle of minimum complementary energy, based on "a priori equilibrated" stress field σ_{ij}inside each element, and an inter-element compatible displacement field $\tilde{u}_i$ along the element boundary, see (59).

$$\pi_6(\sigma_{ij}, u_i) = \sum_m \left\{ \int_{\Omega m} \frac{1}{2} C_{ijkl}\sigma_{ij}\sigma_{kl} d\Omega - \int_{\partial\Omega_m} t_i u_i dS + \int_{S_{tm}} \bar{t}_i u_i dS \right\} \tag{59}$$

Stress modes derived from the Airy stress functions were proposed to be used as the assumed σ_{ij}. For example, the first 12 modes are:

$$\begin{bmatrix} 0 & 0 & 1 & 0 & 0 & x_1 & x_2 & 0 & 0 & x_1^2 & 2x_1x_2 & x_2^2 \\ 1 & 0 & 0 & x_1 & x_2 & 0 & 0 & x_1^2 & 2x_1x_2 & x_2^2 & 0 & 0 \\ 0 & 1 & 0 & 0 & -x_1 & -x_2 & 0 & 0 & -x_1^2 & -2x_1x_2 & -y^2 & 0 \end{bmatrix}$$

And the 13-18 modes are:

$$\begin{bmatrix} 0 & 0 & x_1^3 & 3x_1^2x_2 & 3x_1x_2^2 & x_2^3 \\ x_1^3 & 3x_1^2x_2 & 3x_1x_2^2 & x_2^3 & 0 & 0 \\ 0 & -x_1^3 & -3x_1^2x_2 & -3x_1x_2^2 & -x_2^3 & 0 \end{bmatrix}$$

A necessary condition of the LBB conditions is to select enough stress modes. A frequently used scheme for this type of element is that: for $n \leq 5$, use the first 7 modes; for $n \leq 7$, use the first 12 modes; and for $8 \leq n \leq 10$ use the first 18 modes.

Derived using this two-field variational principle, this type of VCFEM is similar to the hybrid stress elements developed in [Pian (1964)]. In this study, we denote this type of elements as VCFEM-HS-PCE. Because VCFEM-HS-PCE requires numerical integrations for evaluating two matrices (one over the domain, one along the boundary) as well as inverting one, computing the stiffness matrices for each

element is highly inefficient. In addition, Lagrangian multipliers involved in such a two-field variational principle make the derived elements suffer from LBB conditions, which are almost impossible to be satisfied a priori.

In this section, we derive T-Trefftz VCFEMs for micromechanical analysis of heterogeneous materials. A linear displacement $\tilde{u}_i$ along each edge and an interior displacement field u_i are independently assumed. For an arbitrary polygonal element as in Fig. 3 with corresponding nodal displacements $u_i^{(1)}, u_i^{(2)}, ..., u_i^{(n)}$, a linear displacement field along each edge is assumed as:

$$\tilde{u}_i = \sum_{k=1}^{n} \tilde{N}^{(k)}(\mathbf{x}) u_i^{(k)} \text{ at } \partial\Omega_m \text{ assumed linear along each edge} \tag{60}$$

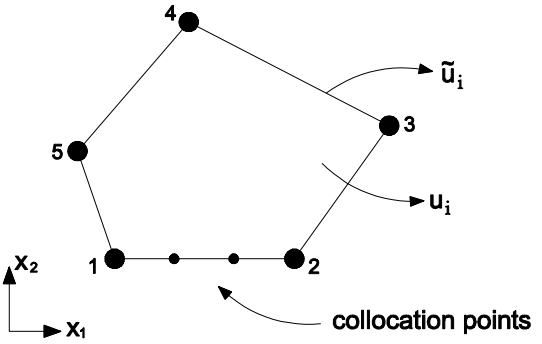

Figure 3: A two-dimensional Voronoi cell finite element

In order to formulate invariant and well-performing elements, an interior displacement field is assumed as a linear combination of the first m T-Trefftz modes derived in section 2, which are complete to a certain order p:

$$\begin{Bmatrix} u_1 & u_2 \end{Bmatrix}^T = \mathbf{T}_0^3\alpha_1 + \mathbf{T}_0^4\alpha_2 + \mathrm{T}_1^1\alpha_3 + ... + \mathbf{T}_p^3 + \mathbf{T}_p^4\alpha_m \text{ in } \Omega_m \tag{61}$$

Obviously, $m = 4p+2 \geq 2n$. u_i includes three rigid-body modes T_0^3, T_0^4, T_1^1 and $4p-1$ non-rigid-body modes. Such an assumption is rotationally invariant itself, so no element-fixed coordinate system is needed to be define in contrast to qudrilateral elements derived in section 3.

Adopting matrix and vector notation, we have:

$$\begin{aligned}
&\mathbf{u} = \mathbf{N}\boldsymbol{\alpha} \text{ in } \Omega_m \\
&\boldsymbol{\varepsilon} = \mathbf{B}\mathbf{q} \text{ in } \Omega_m \\
&\boldsymbol{\sigma} = \mathbf{D}\boldsymbol{\varepsilon} = \mathbf{S}\boldsymbol{\alpha} \text{ in } \Omega_m \\
&\mathbf{t} = \mathbf{n}\boldsymbol{\sigma} = \mathbf{R}\boldsymbol{\alpha} \text{ at } \partial\Omega_m \\
&\tilde{\mathbf{u}} = \tilde{\mathbf{N}}\mathbf{q} \text{ in } \Omega_m
\end{aligned} \tag{62}$$

Similar to the four-node quadrilateral element, there are at least three ways of relating $\boldsymbol{\alpha}$ to $\mathbf{q}$: using the two-field boundary variational principle, or collocation, or the least squares method. However, because $\tilde{\sigma}_{ij}$ are not defined inside Ω_m unlike the four-node quadrilateral element, one cannot enforce the compatibility of $\tilde{\sigma}_{ij}$ and σ_{ij} using collocation or the least squares method. Therefore, we have the following three approaches of developing T-Trefftz VCFEMs.

Firstly, we can substitute assumed $u_i, \tilde{u}_i$ into the two-field boundary variational principle (21). Finite element equations derived in this way are:

$$\sum_m \left(\delta\mathbf{q}^T\mathbf{K}\mathbf{q} - \delta\mathbf{q}^T\mathbf{Q}\right) = \sum_m \left(\delta\mathbf{q}^T\mathbf{G}^T\mathbf{H}^{-1}\mathbf{G}\mathbf{q} - \delta\mathbf{q}^T\mathbf{Q}\right) = 0 \tag{63}$$

where

$$\begin{aligned}
\mathbf{G} &= \int_{\partial\Omega m} \mathbf{R}^T\tilde{\mathbf{N}}dS \\
\mathbf{H} &= \int_{\partial\Omega m} \mathbf{R}^T\mathbf{N}dS = \int_{\Omega m} \mathbf{S}^T\mathbf{D}^{-1}\mathbf{S}^T d\Omega \\
\mathbf{Q} &= \int_{Stm} \tilde{\mathbf{N}}^T\bar{\mathbf{t}}dS
\end{aligned} \tag{64}$$

From a weighted-residual point of view, using boundary variational principle (21), $\boldsymbol{\alpha}$ are related to $\mathbf{q}$ by enforcing the compatibility of u_i and $\tilde{u}_i$ using test function $\delta\mathbf{t} = \mathbf{R}\delta\boldsymbol{\alpha}$. Therefore, rigid-body modes T_0^3, T_0^4, T_1^1 should be eliminated from the assumed u_i.

We denote this type of VCFEM as VCFEM-TT-BVP. VCFEM-TT-BVP is clearly plagued by LBB conditions.

Secondly, we can enforce the compatibility of u_i and $\tilde{u}_i$ at a set of preselected collocation points $x_i^{(k)}, k = 1,2...M$ along $\partial\Omega_m$, see Fig. 3. We obtain:

$$u_i(x_i^{(k)}, \boldsymbol{\alpha}) = \tilde{u}_i(x_i^{(k)}, \mathbf{q}),\ k = 1,2,...,M \tag{65}$$

Relating $\boldsymbol{\alpha}$ to $\mathbf{q}$ by (65), and substituting u_i to variational principle (31), we obtain:

$$\boldsymbol{\alpha} = \mathbf{C}\mathbf{q} \tag{66}$$

$$\sum_m \left(\delta \mathbf{q}^T \mathbf{K}\mathbf{q} - \delta \mathbf{q}^T \mathbf{Q}\right) = \sum_m \left(\delta \mathbf{q}^T \mathbf{C}^T \mathbf{H}\mathbf{C}\mathbf{q} - \delta \mathbf{q}^T \mathbf{Q}\right) = 0 \tag{67}$$

We denote this type of element as VCFEM-TT-C.

Finally, when the number of collocation points is increased to a limit of infinity, it is equivalent to enforce the compatibility between u_i and $\tilde{u}_i$using the least squares method, namely minimizing the following functional:

$$\begin{aligned} e_1(\boldsymbol{\alpha}, \mathbf{q}) &= \int_{\partial\Omega_m} (u_i - \tilde{u}_i)(u_i - \tilde{u}_i) dS \\ &= \int_{\partial\Omega_m} \left(\boldsymbol{\alpha}^T \mathbf{N}^T \mathbf{N}\boldsymbol{\alpha} - 2\boldsymbol{\alpha}^T \mathbf{N}^T \tilde{\mathbf{N}}\mathbf{q} + \mathbf{q}^T \tilde{\mathbf{N}}^T \tilde{\mathbf{N}}\mathbf{q}\right) dS \\ &= \boldsymbol{\alpha}^T \mathbf{U}_1 \boldsymbol{\alpha} - 2\boldsymbol{\alpha}^T \mathbf{V}_1 \mathbf{q} + \mathbf{q}^T \mathbf{W}_1 \mathbf{q} \end{aligned} \tag{68}$$

To minimize e_1 for a fixed $\mathbf{q}$, we have:

$$\boldsymbol{\alpha} = \mathbf{L}\mathbf{q} \tag{69}$$

Substituting u_i into (31), we obtain finite element equations:

$$\sum_m \left(\delta \mathbf{q}^T \mathbf{K}\mathbf{q} - \delta \mathbf{q}^T \mathbf{Q}\right) = \sum_m \left(\delta \mathbf{q}^T \mathbf{L}^T \mathbf{H}\mathbf{L}\mathbf{q} - \delta \mathbf{q}^T \mathbf{Q}\right) = 0 \tag{70}$$

We denote this type of element as VCFEM-TT-LS.

Now that the formulations of all three types of VCFEM-TTs have been developed, we should define m, the number of T-Trefftz modes that should be adopted. Since we use T-Trefftz modes complete to a certain order, this is equivalent to define p, the order that the T-Trefftz modes are complete to. In order to ensure rank-sufficiency, obviously $4p-1$, the number of non-rigid body modes for u_i should be equal or larger than $2n-3$. Therefore, the least-order p to be used are $\left\lceil \frac{2n-2}{4} \right\rceil$, where $\lceil \rceil$ is the function to round a number up to a integer. This means, we use $p=2$ for $n=4,5$, $p=3$ for $n=6,7$, $p=4$ for $n=8,9$.

However, it should be noted that $4p-1 \geq 2n-3$ is only a necessary condition of LBB conditions. It cannot ensure that VCFEM-TT-BVP developed using the least-order T-Trefftz modes are stable. In this study, we also try another larger number for p, $p = \left\lceil \frac{2n+2}{4} \right\rceil$. This is to use $p=3$ for $n=4,5$, $p=4$ for $n=6,7$, $p=5$ for $n=8,9$.

For VCFEM-TT-C, one also needs to select the number of collocation points. In order to ensure the number of collocation equations to be equal or larger than the number of T-Trefftz modes, in this study, we collocate at the points for the two-point Gauss quadrature along each edge. In this way, it is ensured that $2M \geq m = 4p+2$.

5 Numerical Examples

We compare the performance of different elements by conducting numerical experiments. In section 5.1, 5.2 and 5.3, we present numerical examples for four-node quadrilateral elements without drilling DOFs, four-node quadrilateral elements with drilling DOFs, and VCFEMs respectively. All codes are programed using MATLAB in a 64-bit WINDOWS operating system, and executed on a PC computer equipped with Intel Q8300 2.5GHZ CPU, and 8G system memory.

5.1 Examples for Four-Node Quadrilateral Elements without Drilling DOFs

In this section, we compare the performances of the following elements:

- Q4: the primal four-node quadrilateral element without drilling DOFs.
- Q4-HE-C: (quad 4-hybrid strain-collocation), the element denoted as HMFEM2-b in [Dong and Atluri (2011)], with independently assumed strain field ε_{ij} and displacement field $\tilde{u}_i$, compatibility of ε_{ij} and $\tilde{u}_{(i,j)}$ enforced by collocation.
- Q4-TT-BVP: T-Trefftz four-node quadrilateral element, with independently assumed boundary displacement field $\tilde{u}_i$ and interior T-Trefftz type of displacement field u_i, compatibility of u_i and $\tilde{u}_i$ enforced by using the two-field boundary variational principle (21). As mentioned in section 3.1, Q4-TT-BVP has the same stiffness matrix of Q4-HS-PCE, the hybrid stress element developed by [Pian (1964)].
- Q4-TT-C1: T-Trefftz four-node quadrilateral element, compatibility of u_i and $\tilde{u}_i$ enforced by by collocation, finite element equations developed using variational principle (31).
- Q4-TT-C2: T-Trefftz four-node quadrilateral element, compatibility of σ_{ij} and $\tilde{\sigma}_{ij}$ enforced by collocation.
- Q4-TT-LS1: T-Trefftz four-node quadrilateral element, compatibility of u_i and $\tilde{u}_i$ enforced by using the least squares method.
- Q4-TT-LS2: T-Trefftz four-node quadrilateral element, compatibility of σ_{ij} and $\tilde{\sigma}_{ij}$ enforced using the least squares method.

Firstly, we evaluate the eigenvalues of stiffness matrices of a square as well as a distorted element, shown in Fig. 4. Plane stress case is considered. Material properties are $E = 1, v = 0.25$, The coordinates of the square element in the original global Cartesian coordinate system are $(-1,-1),(1,-1),(1,1),(-1,1)$. The

coordinates of the distorted element are $(-1,-1),(1,-1),(2,1),(1,1)$. Then, the stiffness matrices and their corresponding eigenvalues are computed again, in a global Cartesian coordinate system obtained by rotating the original global Cartesian coordinate system with respect to $\mathbf{e_3}$ counterclockwise 45°. As expected, these eigenvalues do not change together with the change of global coordinate system, and they are shown in Tab. 1 and Tab. 2.

From Tab.1 and Tab. 2, we can see that all the elements are rank-sufficient, except for Q4-TT-BVP, which are plagued by LBB conditions. *We mentioned that in section 3.1, Q4-TT-BVP has the same stiffness matrix of Q4-HS-PCE, the hybrid stress element used in [Pian (1964)] and many more studies afterwards. This element has been mistakenly thought to be able to satisfy LBB conditions, simply because the stiffness matrix of a square element is rank-sufficient. However, from Tab. 2, it is clear that rank-sufficiency is not ensured for an arbitrarily-distorted element. To the best of the authors' knowledge, there is no rational way of satisfying LBB conditions a priori for arbitrarily distorted element. This is why we develop hybrid/mixed elements without involving LBB conditions, such as Q4-HE-C, Q4-TT-C1,2, Q4-TT-LS1,2.*

The CPU time used to compute the stiffness matrices of the distorted element is also shown in Tab. 3, normalized to that of the Q4 element. It can be seen that Q4-HE-C is computationally the most efficient.

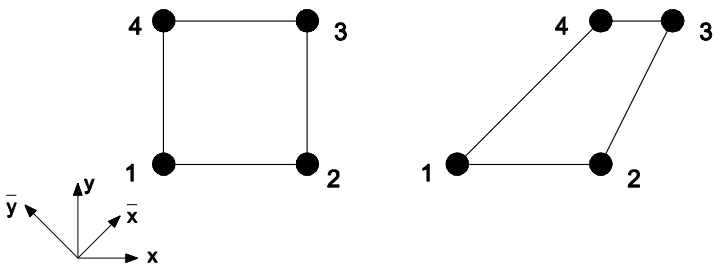

Figure 4: A square and a distorted element for eigenvalue analysis

We also conduct the so-called one-element constant-strain patch test. Plane stress case is considered. The material parameters are taken as $E = 1.0$ and $v = 0.25$. Two type of elements are used for the testing purpose: one is square, and the other is distorted, as shown in Fig. 5. The coordinates of the nodes of the square element is $(-1,0),(1,0),(1,1),(-1,1)$. The coordinates of the nodes of the distorted element is $(-1,0),(1,0),(1,1.5),(-1,1)$. Traction boundary conditions are applied to each edge, except for that the vertical displacements of node 1 and 2 as well as horizontal

Table 1: Eigenvalues of the square element in the original & rotated global Cartesian coordinate system

Eigenvalues Rotation = 0° & 45°	Elements						
	Q4	Q4-HE-C	Q4-TT-BVP	Q4-TT-C1	Q4-TT-C2	Q4-TT-LS1	Q4-TT-LS2
1	1.3333	1.3333	1.3333	1.3333	1.3333	1.3333	1.3333
2	0.8000	0.8000	0.8000	0.8000	0.8000	0.8000	0.8000
3	0.8000	0.8000	0.8000	0.8000	0.8000	0.8000	0.8000
4	0.4889	0.3556	0.3333	0.3333	0.3793	0.2846	0.3793
5	0.4889	0.3556	0.3333	0.3333	0.3793	0.2846	0.3793
6	0.0000	0.0000	0.0000	0.0000	0.0000	0.0000	0.0000
7	0.0000	0.0000	0.0000	0.0000	0.0000	0.0000	0.0000
8	0.0000	0.0000	0.0000	0.0000	0.0000	0.0000	0.0000

Table 2: Eigenvalues of the distorted element in the original & rotated global Cartesian coordinate system

Eigenvalues Rotation =0° & 45°	Elements						
	Q4	Q4-HE-C	Q4-TT-BVP	Q4-TT-C1	Q4-TT-C2	Q4-TT-LS1	Q4-TT-LS2
1	2.7487	2.6875	2.6421	3.4900	2.7743	2.5783	2.6568
2	1.2078	1.1885	1.1791	2.7233	1.2287	1.2119	1.1741
3	0.9169	0.6225	0.4706	0.6579	0.7548	0.4292	0.5084
4	0.5063	0.4600	0.3920	0.4272	0.4271	0.3996	0.4028
5	0.3744	0.3594	0.0000	0.2178	0.3407	0.0979	0.0005
6	0.0000	0.0000	0.0000	0.0000	0.0000	0.0000	0.0000
7	0.0000	0.0000	0.0000	0.0000	0.0000	0.0000	0.0000
8	0.0000	0.0000	0.0000	0.0000	0.0000	0.0000	0.0000

Table 3: CPU time required for computing the stiffness matrix of each element, normalized to that for Q4 element.

CPU Time	Elements						
	Q4	Q4-HE-C	Q4-TT-BVP	Q4-TT-C1	Q4-TT-C2	Q4-TT-LS1	Q4-TT-LS2
	1.00	1.09	1.78	1.47	1.51	2.35	2.01

Table 4: Performances of different elements in the one-element patch test

Element	Elements						
	Q4	Q4-HE-C	Q4-TT-BVP	Q4-TT-C1	Q4-TT-C2	Q4-TT-LS1	Q4-TT-LS2
Square	4.5×10^{-16}	5.5×10^{-16}	7.9×10^{-16}	5.6×10^{-16}	9.8×10^{-16}	4.3×10^{-16}	6.6×10^{-16}
Distorted	5.7×10^{-16}	6.5×10^{-16}	1.1×10^{-15}	3.1×10^{-1}	8.2×10^{-16}	4.3×10^{-2}	2.4×10^{-16}

displacement of node 1 are specified to be corresponding to the exact solution. The exact solution is that of the uniform tension problem:

$$\begin{aligned} u_x &= -\frac{P\bar{v}}{\overline{E}}x \\ u_y &= \frac{P}{\overline{E}}y \end{aligned} \tag{71}$$

where

$$\overline{E} = \begin{cases} E & \\ E/(1-v^2) & \end{cases} \qquad \bar{v} = \begin{cases} v & \text{for plane stress} \\ v/(1-v) & \text{for plane strain} \end{cases} \tag{72}$$

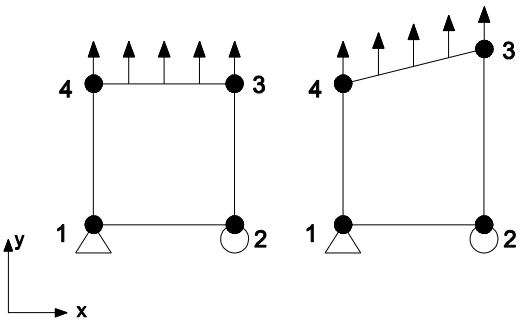

Figure 5: One-element constant-strain patch test

The error is defined as follows:

$$Error = \frac{\|\mathbf{q} - \mathbf{q}^{exact}\|}{\|\mathbf{q}^{exact}\|} \tag{73}$$

where $\mathbf{q}$ and $\mathbf{q}^{exact}$ are the computed and exact nodal displacement vector of the element. And $\|\|$ represents the 2-norm. Experimental results are shown in Tab. 4.

From Tab. 4, one can clearly see that, all the elements can pass the patch test when a square element is used. But for a distorted element is used, Q4-TT-C1 and Q4-TT-LS1 cannot pass the patch test. This is consistent with our analysis in section 3.3.

The performances of different elements are also evaluated, using the problem of a cantilever beam under an end shear load or bending moment. As shown in Fig.

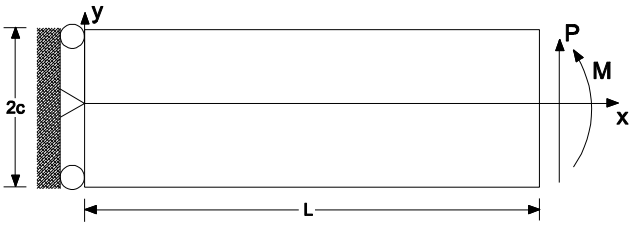

Figure 6: A cantilever beam under an end shear load or bending moment

5, the length and height of the beam is L and $2c$ respectively, and it has a unit thickness. When the beam is under end shear load, the following exact solution is given in [Timoshenko and Goodier (1970)]:

$$\begin{aligned} u_x &= -\frac{Py}{6\overline{E}I}[3x(2L-x)+(2+\overline{\nu})(y^2-c^2)] \\ u_y &= \frac{P}{6\overline{E}I}[x^2(3L-x)+3\overline{\nu}(L-x)y^2+(4+5\overline{\nu})c^2x] \end{aligned} \tag{74}$$

When the beam is under end bending moment, the following exact solution can also be found:

$$\begin{aligned} u_x &= -\frac{M}{\overline{E}I}xy \\ u_y &= \frac{P}{2\overline{E}I}(x^2+\overline{\nu}y^2) \end{aligned} \tag{75}$$

where

$$I = \frac{2c^3}{3} \tag{76}$$

Plane stress case is considered with geometry $L = 10$, $c = 1$, material properties $E = 1.0$ and $\nu = 0$. The distortion ratio is defined as $2e/L$, as can be seen in Fig. 7. Computed vertical displacement is evaluated at tip point A, and normal stress is evaluated at the lower left Gaussian integration point B (2 by 2 rule) of the leftmost element. The computed results are compared to the exact solution, and plotted in Fig. 8-9, with an end unit shear load. When the beam is subject to end unit bending moment, computational results are evaluated at the same points, and plotted in Fig. 10-11. Because Q4-TT-LS1 performs so badly that the error is almost larger than 50% for every distortion ratio, it is not plotted here.

As can be clearly seen in Fig. 8-11, Q4 is always performing badly because of locking. Q4-HE-C, Q4-TT-BVP, Q4-TT-C2 and Q4-TT-LS2 all perform similarly,

which is much better than the performance of the primal Q4 element. Q4-TT-C1 performs very well in this cantilever beam problem. For bending case, Q4-TT-C1 can always give the exact solution.

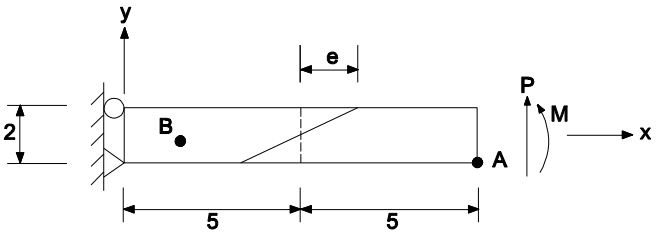

Figure 7: Test of element locking and sensitivity to distortion, cantilever beam under an end shear load or bending moment

From the results presented in this section, we conclude that Q4-TT-BVP is not recommended because it is plagued by LBB conditions. For an arbitrarily distorted element, Q4-TT-BVP may produce rank-deficient stiffness matrix. Q4-TT-LS1 should not be used because it can neither perform well in the in-plane bending problem nor pass the patch test. Careful attention should be paid when using Q4-TT-C1. It performs extraordinarily in the bending problem, but it produces relatively larger error in the patch test when the element is distorted. Q4-HE-C, Q4-TT-C2, Q4-TT-LS2 are not plagued by LBB conditions, can pass the one element patch test, and perform well in the bending problem. Because Q4-TT-LS2 is computationally more expensive than the other two, Q4-HE-C and Q-TT-C2 should be recommended for engineering applications.

5.2 Examples for Four-Node Quadrilateral Elements with Four Drilling DOFs

In this section, we compare the performances of the following elements:

- Q4-D4: the four-node quadrilateral element with four drilling DOFs, independently assumed displacement field $\tilde{u}_i$ and rotation field θ, developed directly using variational principle (38).
- Q4-D4-TT-BVP: T-Trefftz four-node quadrilateral element with four drilling DOFs, with independently assumed interior displacement field u_i as a linear combination of T-Trefftz modes, compatibility of u_i and $\tilde{u}_i$ enforced using variational principle (43).
- Q4-D4-TT-C1: T-Trefftz four-node quadrilateral element with four drilling

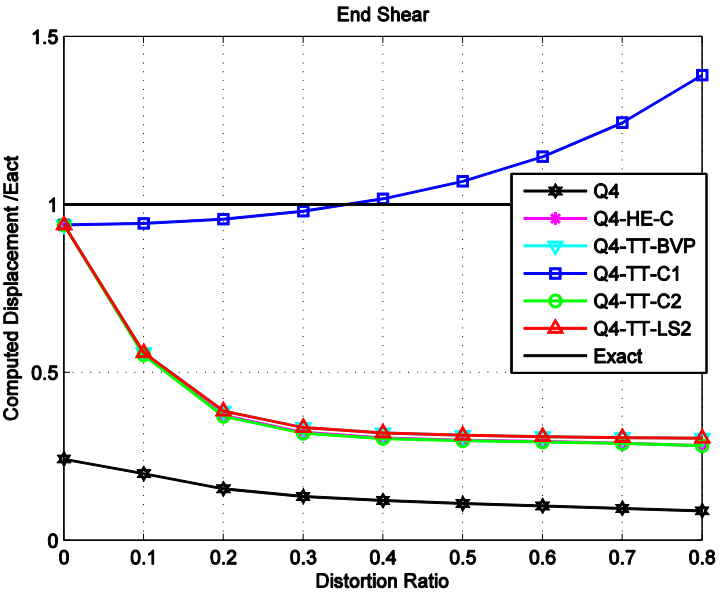

Figure 8: Computed vertical displacement of cantilever beam in Fig. 7 under end shear using elements without drilling DOFs

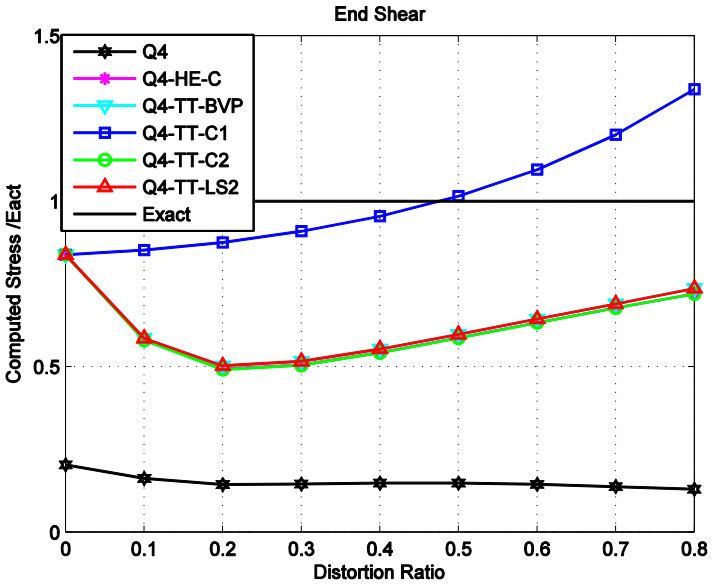

Figure 9: Computed normal stress of cantilever beam in Fig. 7 under end shear using elements without drilling DOFs

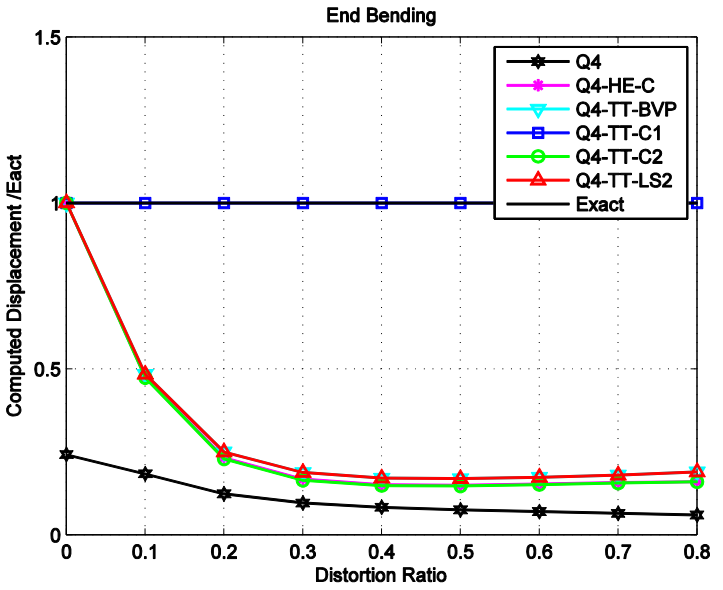

Figure 10: Computed vertical displacement of cantilever beam in Fig. 7 under end bending using elements without drilling DOFs

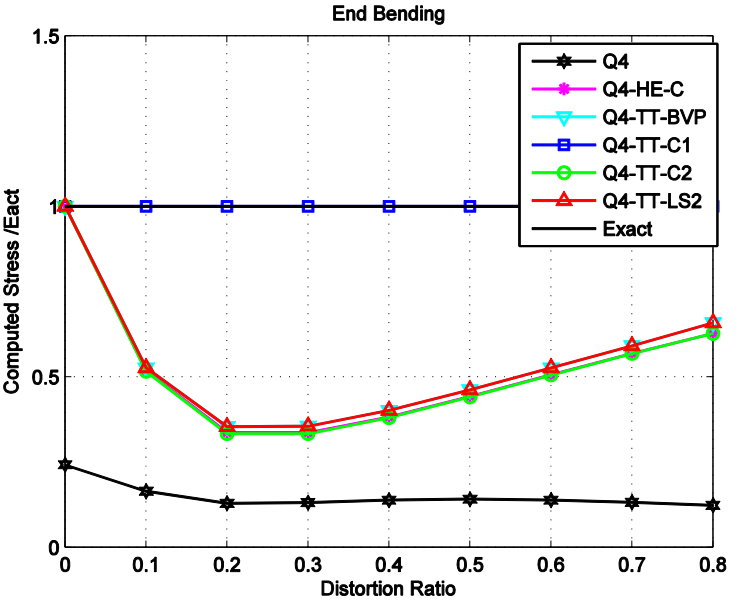

Figure 11: Computed normal stress of cantilever beam in Fig. 7 under end bending using elements without drilling DOFs

DOFs, compatibility of u_i and $\tilde{u}_i$ enforced by collocation, finite element equations developed using variational principle (38).

- Q4-D4-TT-C2: T-Trefftz four-node quadrilateral element with four drilling DOFs, compatibility of σ_{ij} and $\tilde{\sigma}_{ij}$ enforced by collocation.

- Q4-D4-TT-LS1: T-Trefftz four-node quadrilateral element with four drilling DOFs, compatibility of u_i and $\tilde{u}_i$ enforced by using the least squares method.

- Q4-D4-TT-LS2: T-Trefftz four-node quadrilateral element with four drilling DOFs, compatibility of σ_{ij} and $\tilde{\sigma}_{ij}$ enforced using the least squares method.

Firstly, we evaluate the eigenvalues of stiffness matrices of a square as well as a distorted element, using the same elements in Fig. 4. This is, again, conducted in the original and the rotated global Cartesian coordinate system. These eigenvalues are invariant, and they are shown in Tab. 5 and Tab. 6. As can be seen, for these two elements, all approaches give rank-sufficient stiffness matrices. However, similar to Q4-TT-BVP, this does not mean that LBB conditions are satisfied by Q4-D4-TT-BVP. And there is no guarantee that Q4-D4-TT-BVP gives rank-sufficient stiffness matrices for an arbitrarily distorted element.

The CPU time used to compute the stiffness matrices of the distorted element with drilling DOFs is also shown in Tab. 7, normalized to that of the Q4-D4 element.

We also conduct the so-called one-element patch test using the same problem defined in Fig 5. It should be noted that, because none of the drilling DOFs are fixed, according to the definition of the force vector, there should be a nodal moment applied to each node.

The computed results are shown in Tab. 8. Similar results to that of four-node quadrilateral elements without drilling DOFs are obtained. Among these elements, Q4-D4, Q4-D4-TT-BVP, Q4-D4-TT-LS2 can always pass the patch test. Q4-D4-TT-C2 can pass the patch test when an undistorted element is used, and gives very small error when a distorted element is used. Q4-D4-TT-C1 and Q4-D4-TT-LS1 gives relatively large error.

The performances of different elements are also evaluated, using the problem of a cantilever beam under an end shear load or bending moment, as shown in Fig. 6. The computed results are compared to the exact solution, and plotted in Fig. 12-15. From the computed results, one can see that all the T-Trefftz elements give better performances than Q4-D4. Among these elements, Q4-D4-TT-LS1 seems give the best performance. Q4-D4-TT-LS2 gives slightly better performance than that of Q4-D4-TT-BVP and Q4-D4-TT-C2.

Table 5: Eigenvalues of the square element with drilling DOFs in the original & rotated global Cartesian coordinate system

Eigenvalues Rotation=0˚&45˚ = 0˚ & 45˚	Elements					
	Q4-D4	Q4-D4-TT-BVP	Q4- D4-TT-C1	Q4- D4-TT-C2	Q4- D4-TT-LS1	Q4- D4-TT-LS2
1	1.3333	1.3333	1.3333	1.3333	1.3333	1.3333
2	0.9867	0.9862	0.9862	0.9831	0.9844	0.9874
3	0.8000	0.8000	0.8000	0.8000	0.8000	0.8000
4	0.5604	0.4298	0.4540	0.4200	0.4330	0.4200
5	0.5604	0.4298	0. 4540	0.4200	0.4330	0.4200
6	0.3000	0.3000	0.3000	0.3000	0.3000	0.3000
7	0.0952	0.0884	0.0963	0.0563	0.0915	0.0563
8	0.0952	0.0884	0.0963	0.0563	0.0915	0.0563
9	0.0384	0.0361	0.0361	0.0231	0.0381	0.0410
10	0.0000	0.0000	0.0000	0.0000	0.0000	0.0000
11	0.0000	0.0000	0.0000	0.0000	0.0000	0.0000
12	0.0000	0.0000	0.0000	0.0000	0.0000	0.0000

Table 6: Eigenvalues of the distorted element with drilling DOFs in the original & rotated global Cartesian coordinate system

Eigenvalues Rotation = 0° & 45°	Elements					
	Q4-D4	Q4-D4-TT-BVP	Q4- D4-TT-C1	Q4- D4-TT-C2	Q4- D4-TT-LS1	Q4- D4-TT-LS2
1	2.9940	2.9280	2.9413	3.0215	2.9321	2.9491
2	1.3817	1.3720	1.4459	1.3652	1.3739	1.3664
3	1.1690	0.6635	0.7561	0.9512	0.6971	0.9192
4	0.5706	0.5269	0.5202	0.5322	0.5026	0.5408
5	0.4039	0.3918	0. 3659	0.4100	0.3720	0.3970
6	0.2601	0.2115	0.2095	0.2114	0.2109	0.2123
7	0.2112	0.1233	0.1662	0.1617	0.1218	0.1613
8	0.0705	0.0427	0.0321	0.0148	0.0344	0.0532
9	0.0254	0.0184	0.0205	0.0068	0.0185	0.0058
10	0.0000	0.0000	0.0000	0.0000	0.0000	0.0000
11	0.0000	0.0000	0.0000	0.0000	0.0000	0.0000
12	0.0000	0.0000	0.0000	0.0000	0.0000	0.0000

Table 7: CPU time required for computing the stiffness matrix of each element with drilling DOFs, normalized to that for Q4-D4 element.

CPU Time	Elements					
	Q4-D4	Q4-D4-TT-BVP	Q4-D4-TT-C1	Q4-D4-TT-C2	Q4-D4-TT-LS1	Q4-D4-TT-LS2
	1.00	1.69	1.32	1.29	1.88	1.78

Table 8: Performances of different elements with drilling DOFs in the one-element patch test

Element	Elements					
	Q4-D4	Q4-D4-TT-BVP	Q4-D4-TT-C1	Q4-D4-TT-C2	Q4-D4-TT-LS1	Q4-D4-TT-LS2
Square	1.4×10^{-15}	1.4×10^{-15}	8.8×10^{-16}	1.6×10^{-15}	2.0×10^{-2}	1.7×10^{-15}
Distorted	1.3×10^{-15}	1.5×10^{-15}	4.2×10^{-2}	1.4×10^{-2}	4.4×10^{-2}	3.4×10^{-15}

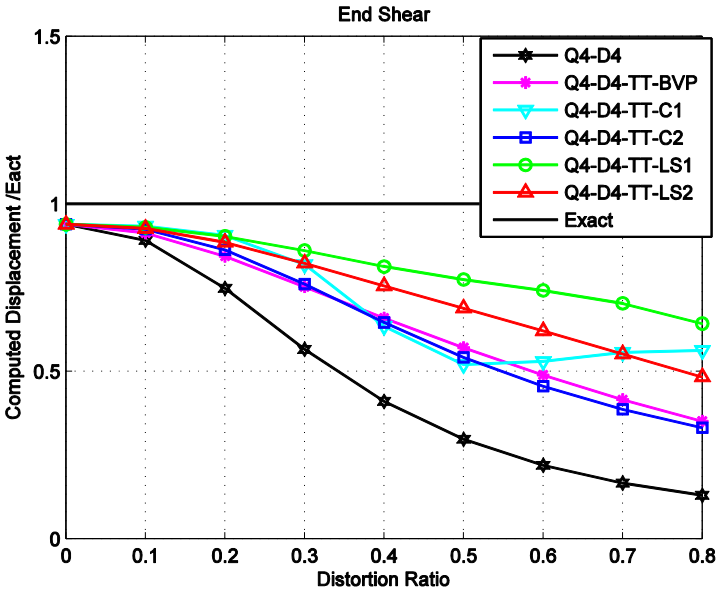

Figure 12: Computed vertical displacement of cantilever beam in Fig. 7 under end shear using elements with drilling DOFs

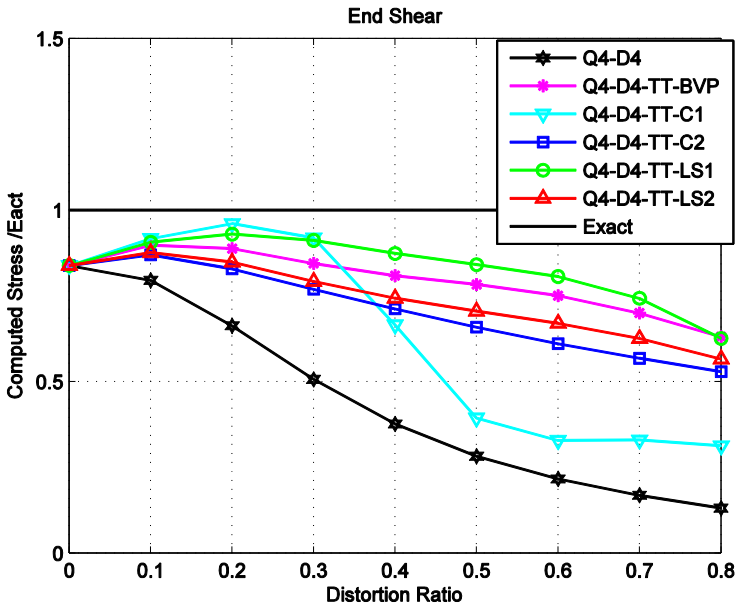

Figure 13: Computed normal stress of cantilever beam in Fig. 7 under end shear using elements with drilling DOFs

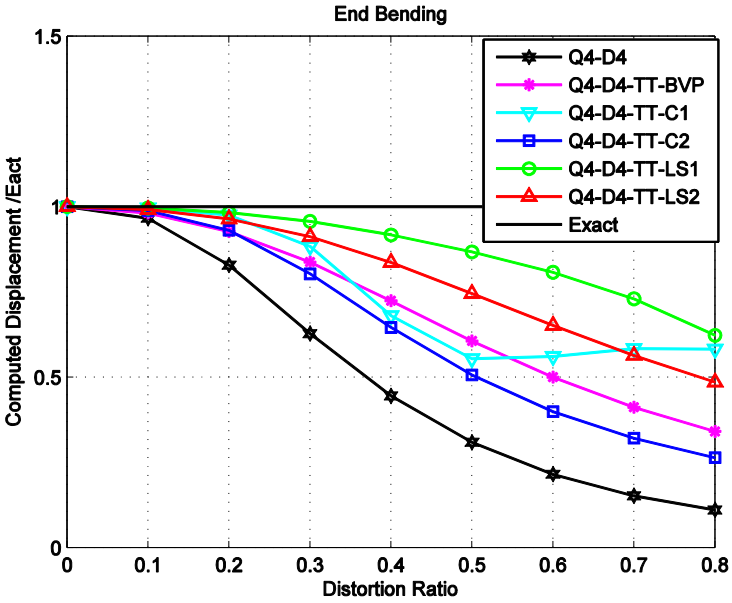

Figure 14: Computed vertical displacement of cantilever beam in Fig. 7 under end bending using elements with drilling DOFs

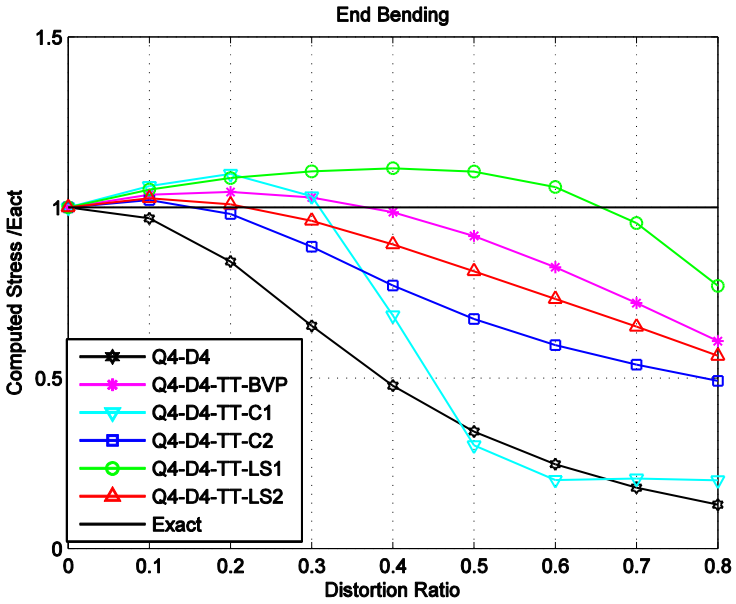

Figure 15: Computed normal stress of cantilever beam in Fig. 7 under end bending using elements with drilling DOFs

From the results presented in this section, we conclude that Q4-TT-C2 and Q4-TT-LS2 should be recommended, because they do not involve LBB conditions, can pass the patch test or give very small error, and perform well in the in-plane bending problem.

5.3 Examples for Voronoi Cell Finite Elements

In this section, we compare the performances of the following elements:

- VCFEM-HS-PCE: Hybrid-stress type of Voronoi cell element used in [Ghosh and Mallett (1994)], with independently assumed boundary displacement field $\tilde{u}_i$ and interior stress field σ_{ij}, developed using the modified principle of complementary energy (59).
- VCFEM-TT-BVP: T-Trefftz Voronoi cell finite element, with independently assumed boundary displacement field $\tilde{u}_i$ and interior T-Trefftz type of displacement field u_i, compatibility of u_i and $\tilde{u}_i$ enforced by using the two-field boundary variational principle (21).
- VCFEM-TT-C: T-Trefftz Voronoi cell finite element, compatibility of u_i and $\tilde{u}_i$ enforced by collocation, finite element equations derived using the variational principel (31).
- VCFEM-TT-LS: T-Trefftz Voronoi cell finite element, compatibility of u_i and $\tilde{u}_i$ enforced using the least squares method, finite element equations derived using the variational principle (31).

As mentioned in section 4, two different values are used for p, which is the order T-Trefftz modes are compete to. They are $p = \left\lceil \frac{2n-2}{4} \right\rceil$ and $p = \left\lceil \frac{2n+2}{4} \right\rceil$.

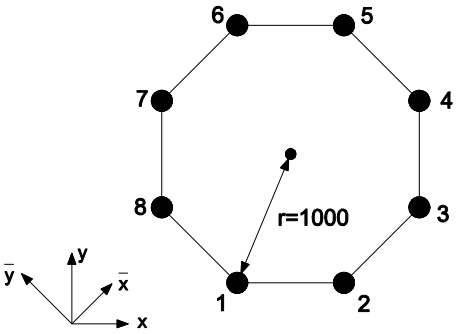

Figure 16: An octagonal element

Firstly, we illustrate the reason why we use a characteristic length to scale the T-Trefftz modes. Plane stress problems with $E = 1$ and $v = 0.25$ are considered. A regular octagonal element with radius 1000 is used, see Fig. 16. We compute the condition number of the coefficient matrices of the equations used to relate $\boldsymbol{\alpha}$ to $\mathbf{q}$. Two cases are considered: (1) T-Trefftz modes are properly scaled with characteristic length $R_c = 1000$; (2) without scaling, which is equivalent to using $R_c = 1$. For simplicity of illustration, only $p = \left\lceil \frac{2n-2}{4} \right\rceil$ is used. Numerical results are shown in Tab. 9. We can clearly see that by scaling the T-complete functions using $R_c = 1000$, the resulting systems of equations have significantly smaller condition number. In the following examples, the characteristic length as defined in (12) is always used.

Using the same octagonal element shown in Fig. 16, we compute the eigenvalues of element stiffness matrices of different VCFEMs. This is conducted in the original and rotated global Cartesian coordinate system. The eigenvalues obviously are invariant with respect to the global coordinate system. Different numbers of p are used, and experimental results are recorded in Tab. 10 and 11 respectively.

As can clearly be seen, these elements are stable and invariant for this regular element. And as larger numbers of T-Trefftz modes are used, the ratio of the largest and smallest non-zeros eigenvalue is increased. This indicates increased stability. However, this does not mean that LBB conditions are satisfied by VCFEM-TT-BVP for an arbitrary element (and VCFEM-HS-PCE). Similar to Q4-TT-BVP as shown in section 5.1, for an arbitrarily distorted element, the stiffness matrix of VCFEM-TT-BVP may be rank-deficient. On this point, VCFEM-TT-C and VCFEM-TT-LS, which do not involve LBB conditions, demonstrate significant advantages.

We also compare the CPU time required for computing the octagonal element in Fig. 9, using different types of elements and different values for p. The CPU time required for each element is normalized to that for VCFEM-HS-PCE, and is listed in Tab. 12. As can be seen, VCFEM-TT-C is computationally the most efficient. And as p is increased, the computational burden is only slightly increased. All the VCFEM-TTs are computationally more efficient than VCFEM-HS-PCE, the elements developed by [Ghosh and Mallett (1994)].

We also conduct the one-element patch test. A pentagonal element with nodal coordinates $(-1,-1),(1,-1),(1,1),(0,2.5),(-1,-1)$ is considered. A shown in Fig. 17, a uniform traction is applied to the upper edge. The vertical displacement of node 1 and 2 are fixed to the exact solution. The horizontal displacement of node 1 is also fixed to the exact solution. The exact solution is shown in (71). The numerical result of different elements using different values of p is shown in Tab. 13. As can be seen, VCFEM-HS and VCFEM-TT-BVP can always pass the patch test. Although the other two types of VCFEMs cannot exactly reproduce the linear field,

Table 9: Condition number of coefficient matrices of equations used to relate $\boldsymbol{\alpha}$ to $\mathbf{q}$ with/without introducing proper characteristic length, $p = \lceil \frac{2n-2}{4} \rceil$

Elements	VCFEM-TT-BVP		VCFEM-TT-C		VCFEM-TT-LS	
Characteristic length	R_c=1000	R_c=1	R_c=1000	R_c=1	R_c=1000	R_c=1
Condition number	84.3	1.3×10^{19}	9.4	6.3×10^{12}	82.6	4.0×10^{25}

Table 10: Eigenvalues of stiffness matrices of different VCFEM-TTs when $p = \lceil \frac{2n-2}{4} \rceil$

Eigenvalues Rotation = 0° & 45°	VCFEM-TT-BVP	VCFEM-TT-C	VCFEM-TT-LS
1	0.9428	0.9428	0.9428
2	0.8121	0.8334	0.8295
3	0.8121	0.8334	0.8295
4	0.6733	0.7649	0.7415
5	0.6733	0.7649	0.7415
6	0.5657	0.5657	0.5657
7	0.5657	0.5657	0.5657
8	0.5170	0.4714	0.5164
9	0.5170	0.4714	0.5164
10	0.3691	0.3788	0.3756
11	0.3691	0.3788	0.3756
12	0.3051	0.3488	0.3351
13	0.3051	0.3488	0.3351
14	0.0000	0.0000	0.0000
15	0.0000	0.0000	0.0000
16	0.0000	0.0000	0.0000

errors for VCFEM-TT-C and VCFEM-TT-LS can be made satisfactorily small by using a slightly larger number of T-Trefftz modes. As can be seen in Tab. 13, when $p = \lceil \frac{2n+2}{4} \rceil$ is used, the numerical errors for both VCFEM-TT-C and VCFEM-TT-LS are both less than 1%.

We also evaluate the performance of VCFEMs by modeling the cantilever beam with mesh configuration shown in Fig. 18, and compare their performances to the exact solution. Geometry properties$L = 10$, $c = 1$, material properties $E = 1500$ and $v = 0.25$ are used. Two loading cases are considered: end shear load $P = 300$ and end bending moment$M = 2000$. The mesh configuration includes 10 elements. Appropriate displacement and traction boundary conditions are applied to the left side and right side of the beam. Computed tip vertical displacement at point A, and normal stress at lower left corner are shown in Tab. 14. From this example, we can see that using either values for p, similar or better performances can be obtained by VCFEM-TTs than that of VCFEM-HS-PCE.

We also compare different VCFEMs by determining the homogenized elastic material properties of functionally graded materials (FGM). Ni_3Al/TiC FGM is consid-

Table 11: Eigenvalues of stiffness matrices of different VCFEM-TTs when $p = \lceil \frac{2n+2}{4} \rceil$

Eigenvalues Rotation = 0° & 45°	VCFEM-TT-BVP	VCFEM-TT-C	VCFEM-TT-LS
1	0.9428	0.9428	0.9428
2	0.8121	0.8334	0.8295
3	0.8121	0.8334	0.8295
4	0.7305	0.6899	0.7307
5	0.7136	0.6892	0.7128
6	0.5657	0.5657	0.5657
7	0.5657	0.5657	0.5657
8	0.5170	0.4714	0.5164
9	0.5170	0.4714	0.5164
10	0.4140	0.3840	0.4127
11	0.4140	0.3840	0.4127
12	0.3691	0.3788	0.3756
13	0.3691	0.3788	0.3756
14	0.0000	0.0000	0.0000
15	0.0000	0.0000	0.0000
16	0.0000	0.0000	0.0000

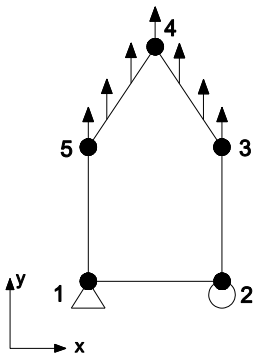

Figure 17: A pentagonal element used for patch test

ered where volume fractions of both materials are 50%. A representative volume element with 300 VCFEMs is used where the distribution of materials in this RVE is randomly generated see Fig. 19. Young's modulus and Poisson's ratio of Ni_3Al and TiC are taken as follows:$E_{Ni_3Al} = 217GPa, \nu_{Ni_3Al} = 0.30; E_{TiC} = 440GPa, \nu_{TiC} =$

Table 12: CPU time required for computing the stiffness matrix of different VCFEMs for different values of p

CPU Time		VCFEM-TT-BVP	VCFEM-TT-C	VCFEM-TT-LS	VCFEM-HS-PCE
p	$\lceil\frac{2n-2}{4}\rceil$	0.75	0.68	0.81	1.00
	$\lceil\frac{2n+2}{4}\rceil$	0.78	0.69	0.85	

Table 13: Performances of different VCFEMs in the constant strain patch test

Error		VCFEM-TT-BVP	VCFEM-TT-C	VCFEM-TT-LS	VCFEM-HS-PCE
p	$\lceil\frac{2n-2}{4}\rceil$	3.6×10^{-16}	6.5×10^{-2}	6.2×10^{-2}	5.1×10^{-16}
	$\lceil\frac{2n+2}{4}\rceil$	4.6×10^{-16}	6.8×10^{-3}	1.9×10^{-3}	

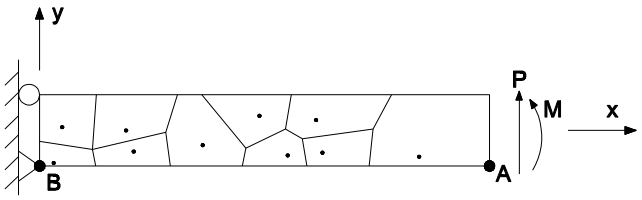

Figure 18: Mesh configuration used for overall test of performances of different VCFEMs

Table 14: Computed and exact solution of cantilever beam in Fig. 5 under end shear or bending moment

p	Element Type	End Shear		End Bending	
		v_A	σ_B	v_A	σ_B
$\lceil\frac{2n-2}{4}\rceil$	VCFEM-TT-BVP	89.6	3843.4	86.4	2696.5
	VCFEM-TT-C	91.1	4204.4	87.6	2940.4
	VCFEM-TT-LS	92.2	4402.2	87.8	3092.5
$\lceil\frac{2n+2}{4}\rceil$	VCFEM-TT-BVP	87.8	3524.5	84.4	2485.5
	VCFEM-TT-C	88.9	3594.1	85.3	2532.4
	VCFEM-TT-LS	89.5	3676.2	85.5	2595.2
VCFEM-HS-PCE		89.6	3843.7	86.4	2696.8
Exact		102.6	4500.0	100.3	3000.0

0.19. The RVE is loaded with a uniform tension in the vertical direction. The homogenized elastic modulus is determined by dividing the tensile force with the extension in the vertical direction. And the homogenized Poisson's ratio is computed as the ratio of the contraction in the horizontal direction and the extension in the vertical direction. Numerical results using different elements are listed in Tab. 15. As can be seen, homogenized material properties using different elements are very close.

From the results presented in this section, we consider that VCFEM-TT-C with $p = \lceil\frac{2n+2}{4}\rceil$ is recommended, because it is computationally efficient, it does not involve LBB conditions, it produces very small error in the path test, and it performs well for the macro-mechanical beam bending problem, and for the problem of determining material properties from an representative volume element.

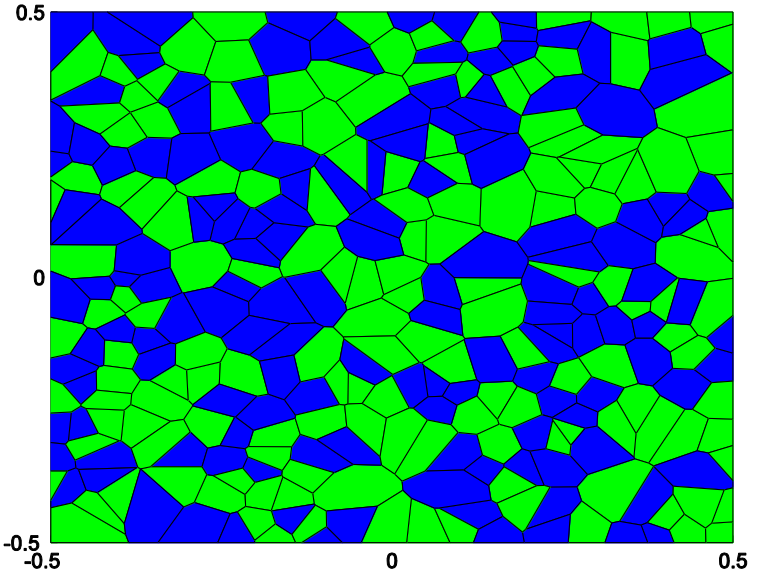

Figure 19: A RVE composed of randomly distributed Ni_3Al and TiC, the green colored patches represent Ni_3Al, the blue colored patches represent TiC

Table 15: Computed material properties of the FGM using the RVE in Fig. 19

p	Element Type	Young's Modulus (GPa)	Poisson's Ratio
$\lceil \frac{2n-2}{4} \rceil$	VCFEM-TT-BVP	304.6	0.2526
	VCFEM-TT-C	303.7	0.2517
	VCFEM-TT-LS	302.6	0.2516
$\lceil \frac{2n+2}{4} \rceil$	VCFEM-TT-BVP	305.3	0.2513
	VCFEM-TT-C	304.9	0.2504
	VCFEM-TT-LS	304.8	0.2512
VCFEM-HS-PCE		304.5	0.2526

6 Conclusion

Three different approaches of developing T-Trefftz elements are explored, by assuming an inter-element compatible displacement field $\tilde{u}_i$ along the element boundary, and an interior displacement field u_i as a linear combination of T-Trefftz modes. Among these three approaches TT-BVP is plagued by LBB conditions, because the two-field boundary variational principle uses Lagrangian multipliers to enforce the compatibility between the independently assumed fields. On the other hand, for

TT-C and TT-LS, because compatibility between independently assumed fields is enforced using either collocation or the least squares method, no LBB conditions are involved.

The corresponding four-node quadrilateral elements with/without drilling degrees of freedoms are also developed. Numerical results show that for T-Trefftz four-node quadrilateral elements without drilling DOFs, Q4-TT-C2, which enforces the compatibility of stress fields derived from u_i and $\tilde{u}_i$ using collocation, should be recommended. This is because it can pass the one-element patch test, it performs well in the in-plane bending problem, it is computationally efficient, and it does not suffer from LBB conditions. For T-Trefftz four-node quadrilateral elements with four drilling DOFs, Q4-D4-TT-C2 and Q4-D4-TT-LS2 should be recommended. While both these two elements do not involve LBB conditions, Q4-D4-TT-LS2 are slightly more accurate than Q4-D4-TT-C2, but computationally more expensive than Q4-D4-TT-C2.

These three approaches are also used to develop Voronoi cell finite elements. VCFEM-TT-BVP, VCFEM-TT-C and VCFEM-TT-LS are developed, which are all shown to have similar performance but be computationally more efficient than the VCFEM-HS-PCE developed by [Ghosh and Mallett (1994); Ghosh, Lee and Moorthy (1995)]. For T-Trefftz Voronoi cell finite elements, VCFEM-TT-C with $p = \left\lceil \frac{2n+2}{4} \right\rceil$ is recommended, because it is computationally efficient, it does not involve LBB conditions, it produces a very small error in the path test, and it performs well in the macro-mechanical beam bending problem, as well as in the problem of determining material properties from an representative volume element.

We conclude this paper by pointing out that, although the present work is conducted in the context of two-dimensional linear elastic solid mechanics, extension to three-dimensional problems and geometrical as well as material nonlinear problems is quite straight-forward. This will be reserved for future study.

Acknowledgement: This work was supported in part by the Vehicle Technology Division of the Army Research Labs, under a collaborative research agreement with University of California, Irvine (UCI), and in part by the Word Class University (WCU) program through the National Research Foundation of Korea, funded by the Ministry of Education, Science and Technology (Grant no.: R33-10049). The first author also would like to thank Professor Masanobu Shinozuka for his kind support of the first author's study.

References

Allman, D. J. (1984): A compatible triangular element including vertex rotations for plane elasticity analysis. *Computers & Structures*, vol. 19, issue 1-2, pp. 23–37.

Atluri, S. N. (1975): On hybrid finite element models in solid mechanics. *Advances in Computer Methods* for *Partial Differential Equations,* R. Vichnevetsky (eds.), AICA, pp. 346-356.

Atluri, S. N. (1980): On some new general and complementary energy theorems for the rate problems in finite Strain, classical elastoplasticity. *Journal of Structural Mechanics,* vol. 8, issue. 1, pp. 61-92.

Atluri, S. N.; Grannel, J. J. (1978): Boundary elements methods and combination of BEM-FEM. Report No. GIT-ESM-SA-78-16.

Babuska, I. (1973): The finite element method with Lagrangian multipliers. *Numerische Mathematik*, vol. 20, no. 3, pp. 179-192.

Bratianu, C.; Atluri, S. N. (1983): A hybrid finite element method for Stokes flow: part I-formulation and numerical studies. *Computer Methods in Applied Mechanics and Engineering*, vol. 36, pp. 23–37.

Brezzi, F. (1974): On the existence, uniqueness and approximation of saddle-point problems arising from Lagrangian multipliers. *Revue Française D'automatique, Informatique, Recherche Opérationnelle, Analyse Numérique*, vol. 8, no. 2, pp. 129-151.

Cai, Y. C.; Paik, J. K.; Atluri, S. N. (2009a): Large deformation analyses of space-frame structures, with members of arbitrary cross-section, using explicit tangent stiffness matrices, based on a von Karman type nonlinear theory in rotated reference frames, *CMES: Computer Modeling in Engineering & Sciences*, vol. 53, no. 2, pp. 117-145.

Cai, Y. C.; Paik, J. K.; Atluri, S. N. (2009b): Large deformation analyses of space-frame structures, using explicit tangent stiffness matrices, based on the Reissner variational principle and a von Karman type nonlinear theory in rotated reference frames. *CMES: Computer Modeling in Engineering & Sciences*, vol. 54, no. 3, pp. 335-368.

Cai, Y. C.; Paik, J. K.; Atluri, S. N. (2010): Locking-free thick-thin rod/beam element for large deformation analyses of space-frame structures, based on the Reissner variational principle and a von Karman type nonlinear theory, *CMES: Computer Modeling in Engineering & Sciences*, vol. 58, no. 1, pp. 75-108.

Cai, Y. C.; Paik, J. K.; Atluri, S. N. (2010): A triangular plate element with drilling degrees of freedom, for large rotation analyses of built-up plate/shell structures, based on the Reissner variational principle and the von Karman nonlinear

theory in the co-rotational reference frame. *CMES: Computer Modeling in Engineering & Sciences*, vol. 61, no. 3, pp. 273-312.

Cazzani, A.; Atluri, S. N. (1993): Four-noded mixed finite elements, using unsymmetric stresses, for linear analysis of membranes. *Computational Mechanics*, vol. 11, no. 4, pp. 229-251.

Dong, L.; Atluri, S. N. (2011): A Simple Procedure to Develop Efficient & Stable Hybrid/Mixed Elements, and Voronoi Cell Finite Elements for Macro- & Micromechanics. CMC: *CMC: Computers, Materials & Continua*, vol. 24, no. 1, pp.61-104.

Ghosh, S.; Mallett, R. L. (1994): Voronoi cell finite elements. *Computers & Structures*, vol. 50, issue 1, pp. 33-46.

Ghosh, S.; Lee, K.; Moorthy, S. (1995): Multiple scale analysis of heterogeneous elastic structures using homogenization theory and Voronoi cell finite element method. *International Journal of Solids and Structures*, vol. 32, issue 1, pp. 27-63.

Iura, M.; Atluri, S. N. (1992): Formulation of a membrane finite element with drilling degrees of freedom. *Computational Mechanics*, vol.9, no. 6, pp.417-428.

Jirousek, J.; Teodorescu, P. (1982): Large finite elements method for the solution of problems in the theory of elasticity. *Computers & Structures*, vol.15, issue. 6, pp.575-587.

Jirousek, J.; Guex, Lan. (1986): The hybrid-Trefftz finite element model and its application to plate bending. *International Journal for Numerical Methods in Engineering*, vol.23, issue. 4, pp.651-693.

Liu, C. S. (2007a): A modified Trefftz method for two-dimensional Laplace equation considering the domain's characteristic length. *CMES: Computer Modeling in Engineering & Sciences*, vol.21, no. 1, pp.53-65.

Liu, C. S. (2007b): An effectively modified direct Trefftz method for 2D potential problems considering the domain's characteristic length. *Engineernig Analysis with Boundary Elements*, vol. 31, issue 12, pp. 983-993.

Muskhelishvili (1954): *Some Basic Problems of the Mathematical Theory of Elasticity*, 4^{th} edition, translated by Radok, Noordhoff, Leyden, The Netherlands, 1975.

Hughes, T. J. R.; Brezzi, F. (1989): On drilling degrees of freedom. *Computer Methods in Applied Mechanics and Engineering*, vol. 72, no. 1, pp. 105-121.

Pian, T. H. H. (1964): Derivation of element stiffness matrices by assumed stress distribution. *A. I. A. A. Journal*, vol. 2, pp. 1333-1336.

Pian, T. H. H.; Chen, D. (1983): On the suppression of zero energy deformation modes. *International Journal for Numerical Methods in Engineering*, vol. 19, issue

12, pp. 1741–1752.

Punch, E. F.; Atluri, S. N. (1984): Development and testing of stable, invariant, isoparametric curvilinear 2- and 3-D hybrid-stress elements. *Computer Methods in Applied Mechanics and Engineering*, vol 47, issue 3, pp. 331-356.

Rubinstein, R.; Punch, E. F.; Atluri, S. N. (1984): An analysis of, and remedies for, kinematic modes in hybrid-stress finite elements: selection of stable, invariant stress fields. *Computer Methods in Applied Mechanics and Engineering*, vol. 38, issue 1, pp. 63-92.

Timoshenko, S. P.; Goodier, J. N. (1976): *Theory of Elasticity*, 3^{rd} edition, McGraw Hill.

Xue, W.; Karlovitz, L. A.; Atluri, S. N. (1985): On the existence and stability conditions for mixed-hybrid finite element solutions based on Reissner's variational principle. *International Journal of Solids and Structures*, vol. 21, issue 1, 1985, pp. 97-116.

Ying, L. A.; Atluri, S. N. (1983): A Hybrid finite element method for Stokes flow: Part II-stability and convergence studies. *Computer Methods in Applied Mechanics and Engineering*, vol. 36, pp. 39–60.

Zhu, H. H.; Cai, Y.C.; Paik, J.K.; Atluri, S. N. (2010): Locking-free thick-thin rod/beam element based on a von Karman type nonlinear theory in rotated reference frames for large deformation analyses of space-frame structures. *CMES: Computer Modeling in Engineering & Sciences*, vol. 57, no. 2, pp. 175-204.